

Multiscale Geometry of the Olsen Model and Non-Classical Relaxation Oscillations

Christian Kuehn* and Peter Szmolyan*

June 8, 2019

Abstract

We study the Olsen model for the peroxidase-oxidase reaction. The dynamics is analyzed using a geometric decomposition based upon multiple time scales. The Olsen model is four-dimensional, not in a standard form required by geometric singular perturbation theory and contains multiple small parameters. These three obstacles are the main challenges we resolve by our analysis. Scaling and the blow-up method are used to identify several subsystems. The results presented here provide a rigorous analysis for two oscillatory modes. In particular, we prove the existence of non-classical relaxation oscillations in two cases. The analysis is based upon desingularization of lines of transcritical and submanifolds of fold singularities in combination with an integrable relaxation phase. In this context our analysis also explains an assumption that has been utilized, based purely on numerical reasoning, in a previous bifurcation analysis by Desroches, Krauskopf and Osinga [Discret. Contin. Dyn. Syst. S, 2(4), p.807–827, 2009]. Furthermore, the geometric decomposition we develop forms the basis to prove the existence of mixed-mode and chaotic oscillations in the Olsen model, which will be discussed in more detail in future work.

Preprint: comments and suggestions welcome!

Keywords: Olsen model, multiple time scales, relaxation oscillation, geometric singular perturbation theory, blow-up method, transcritical singularity, fold singularity, center manifolds, bifurcation delay.

1 Introduction & Review

Experimental observation of oscillatory dynamics [61] in the peroxidase-oxidase (PO) reaction



led to further interest in the dynamical mechanisms [13]. Various models have been proposed [62, 1, 53] to capture the dynamics of (1). We are going to study a model for the PO reaction

*Institute for Analysis and Scientific Computing, Vienna University of Technology, Vienna, 1040, Austria.

initially proposed by Degn, Olsen and Perram [13] (DOP). The four ordinary differential equations (ODEs), as considered by Olsen [60], are

$$\begin{aligned}\frac{dA}{dT} &= -k_3ABY + k_7 - k_{-7}A, \\ \frac{dB}{dT} &= -k_3ABY - k_1BX + k_8, \\ \frac{dX}{dT} &= k_1BX - 2k_2X^2 + 3k_3ABY - k_4X + k_6, \\ \frac{dY}{dT} &= -k_3ABY + 2k_2X^2 - k_5Y,\end{aligned}\tag{2}$$

where $(A, B, X, Y) \in (\mathbb{R}^4)_0^+ = \{(A, B, X, Y) \in \mathbb{R}^4 : A \geq 0, B \geq 0, X \geq 0, Y \geq 0\}$ are chemical concentrations and $k_i > 0$ are parameters. A and B denote concentrations of the substrates $NADH$ and O_2 while X and Y are concentrations for two free radicals. We refer to (2) as the Olsen model.

We briefly describe numerical integration results for the standard parameter values [60]; see Table 1. Olsen used k_1 as a bifurcation parameter and found three main distinct regimes consisting of mixed-mode oscillations (MMOs), chaos and relaxation-type periodic oscillations; see Figure 1. We are going to use the values in Table 1 as the main reference parameter set, where k_1 can take three different values. In this paper, we are primarily interested in periodic oscillations, similar to the results shown in Figure 1(c) for $k_1 = 0.41$. However, we shall already indicate how this regime differs from the other two from the geometric singular perturbation theory (GSPT) viewpoint. Our results on the reduction and the existence of periodic orbits of (2) are stated in Section 2.

| k_1 | k_2 | k_3 | k_4 | k_5 | k_6 | k_7 | k_{-7} | k_8 |
|------------------|-------|-------|-------|-------|-----------|-------|----------|-------|
| 0.16, 0.35, 0.41 | 250 | 0.035 | 20 | 5.35 | 10^{-5} | 0.8 | 0.1 | 0.825 |

Table 1: Standard parameter values for the Olsen model (2).

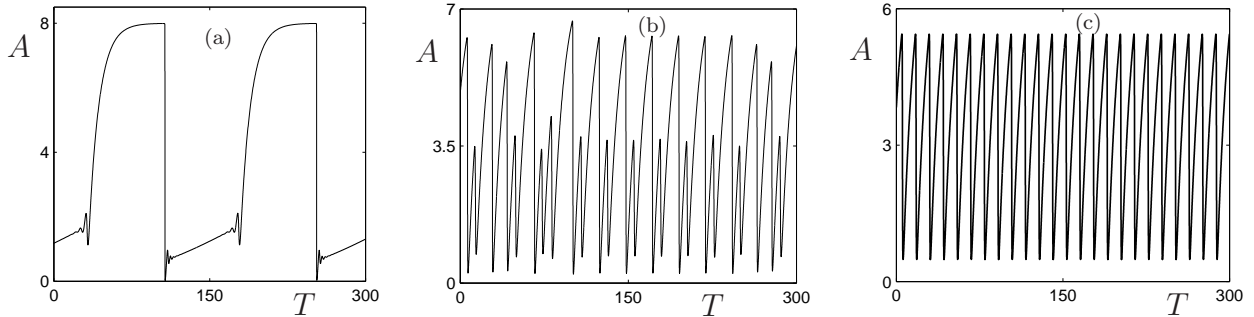


Figure 1: Numerical simulation for (2) with parameter values in Table 1 upon varying k_1 . (a) MMOs for $k_1 = 0.16$, (b) chaotic/aperiodic oscillations for $k_1 = 0.35$ and (c) regular periodic oscillations for $k_1 = 0.41$.

We briefly review previous work on the peroxidase-oxidase reaction as well as the mathematical techniques we use for our analysis. An important starting point are the numerical simulations by Olsen [60] showing that (2) can exhibit various types of oscillations depending on the choice of parameters. Bifurcations of equilibria and sequences of MMOs are investigated in [52]. Considering the chemical reaction mechanisms, it was already realized by

Aguda, Larter and Clarke [2] - based on chemical considerations - that the Olsen model can probably be best understood by decomposition into smaller subsystems. Then various routes to chaos were proposed ranging from torus break-up [54, 68], more detailed reaction mechanisms [1] to classical period-doubling scenarios [67]. Subsequently, MMOs, period-doubling sequences and chaotic dynamics were observed in experiments [31, 32, 23]. Analysis of Lyapunov exponents and period-doubling bifurcations in experimental and numerical simulation time series provided very strong evidence that chaotic dynamics occurs [22, 67]. Thompson and Larter realized the crucial role of multiple time scales in the Olsen model and suggested that a fast-slow variable decomposition is important to understand the oscillations [70]. Multiple time scale structures were also investigated in more detailed models of the PO reaction. For example, it was conjectured in [33] that slow manifolds and homoclinic orbits play an important role; Hopf bifurcations [8, 34] and bursting oscillations were found as well [64, 9] using numerical simulation. Recently, a detailed numerical continuation parameter study was carried out by Desroches, Krauskopf and Osinga [15] who computed various patterns of periodic orbits, MMOs, chaotic dynamics as well as slow manifolds.

Although the reaction-kinetics and the detail of modelling required are still not quite clear [66] it is evident from the results on the Olsen model that oscillations, multiple time scales and decomposition are key aspects. However, the Olsen model has resisted rigorous mathematical analysis for over thirty years, despite it being a key motivating example to study multiple time scale dynamics [56]. In this paper, we provide a first detailed GSPT analysis of the Olsen model to understand the geometry of oscillations. In fact, our analysis also explains why one has not been able to carry out rigorous geometric dissection previously. We establish existence results for several special types of periodic solutions. Furthermore, our analysis provides the basis to prove the existence of chaos generating mechanisms, which will be detailed elsewhere.

The analysis of periodic orbits in multiple time scales systems has an interesting history. The seminal work of van der Pol on relaxation oscillations [72, 73] is one of the main starting points for the interest in fast-slow oscillatory systems. The discovery of “chaotic relaxation oscillations” [10, 11] as well as canard periodic orbits [7, 17] showed that highly complicated dynamics can be obtained from rather simple polynomial fast-slow vector fields. Further analysis revealed that multiple time scale mechanisms can also account for oscillations with special patterns such as MMOs [5] and bursting [63]. For recent reviews on these topics see [14, 37]. It is important to note that often the analysis has been carried out in systems with suitably minimal dimension, where local normal form theory applies, which have a global separation of time scales and which exhibit a return mechanism similar to the original van der Pol system via S-shaped critical manifolds [24, 41, 50]. Although several exceptions of this framework have been considered, for example the general analysis of folded singularities [74], fast-slow systems in non-standard form [43], systems with three time scales [44] and higher-dimensional systems [49, 30] arising in applications, we are still quite far away from understanding high-dimensional multiple time scale dynamics in general systems. The main obstacle for the analysis of the Olsen model is that all problems occur simultaneously. It is four-dimensional, in nonstandard form, contains several non-folded degenerate singularities, has three natural small parameters and a return mechanism without an S-shaped manifold. It even has multiple regimes of different geometric multiple time scale decompositions due

to the relative asymptotic limits of the small parameters. In this paper, we address most of these issues, which are then used to prove the existence of certain periodic solutions.

The main tools we use to analyze the Olsen model are GSPT, desingularization via the blow-up method and bifurcation theory in combination with standard techniques from dynamical systems such as local center manifolds and stability theory. Geometric theory for normally hyperbolic fast-slow systems was initially developed by Tikhonov [71], Fenichel [21] and various other groups [35]; for recent reviews see [38, 39]. For a brief statement of the main result see Appendix A.

The blow-up technique was introduced into fast-slow systems by the seminal work of Dumortier and Roussarie [19]. It has been used to analyze various local singularities such as fold points [45], folded nodes [69], Bogdanov-Takens points [12], intersection points of slow dynamics [46] and many others. It can also be used to help to resolve global phenomena such as canard explosion [48], periodic orbits [28] and homoclinic orbits [36]. Usually blow-up is used for a distinguished small parameter ϵ , but see [42]. Appendix B provides a brief review of the blow-up method.

The paper is structured as follows: In Section 2 we use a rescaling to describe a version of the Olsen model which is the starting point of our analysis. Furthermore, we state our main results. Section 2 ends with a geometric outline for the analysis to follow. In Section 3 we employ the blow-up method to desingularize a submanifold of fold singularities at which the transition between slow drift dynamics and fast large loops takes place. Section 4 is dedicated to a much finer analysis of the slow drift dynamics in a scaling chart of the first blow-up while Section 5 provides the study of the fast large loops. In Section 6 we construct two classes of candidate (or singular limit) trajectories for certain open sets of parameters. In Section 7 all the previous results are combined to obtain the existence of two types of non-classical relaxation oscillations in the Olsen model. An outlook to other oscillatory patterns and chaotic dynamics, and their analysis via GSPT, is provided in Section 8.

2 Transformations and the Main Result

The first step is to scale (2) to get a better understanding of the multiple time scale structure. We use a slight modification of a scaling suggested by Milik [56]

$$A = \frac{k_1 k_5}{k_3 \sqrt{2k_2 k_8}} a_2, \quad B = \frac{\sqrt{2k_2 k_8}}{k_1} b_2, \quad X = \frac{k_8}{2k_2} x_2, \quad Y = \frac{k_8}{k_5} y_2, \quad T = \frac{k_1 k_5}{k_3 k_8 \sqrt{2k_2 k_8}} s,$$

which transforms the Olsen model into

$$\begin{aligned} \frac{da_2}{ds} &= \mu - \alpha a_2 - a_2 b_2 y_2, \\ \frac{db_2}{ds} &= \epsilon_b (1 - b_2 x_2 - a_2 b_2 y_2), \\ \epsilon^2 \frac{dx_2}{ds} &= b_2 x_2 - x_2^2 + 3a_2 b_2 y_2 - \xi x_2 + \delta, \\ \epsilon^2 \frac{dy_2}{ds} &= \kappa (x_2^2 - y_2 - a_2 b_2 y_2), \end{aligned} \tag{3}$$

where $(a_2, b_2, x_2, y_2) \in (\mathbb{R}^4)_0^+$ and the new parameters are given by

$$\begin{aligned} \mu &= \frac{k_7}{k_8}, & \alpha &= \frac{k_1 k_5 k_{-7}}{k_3 k_8 \sqrt{2k_2 k_8}}, & \epsilon_b &= \frac{k_1^2 k_5}{2k_2 k_3 k_8}, & \kappa &= \frac{\sqrt{2k_2 k_8}}{k_5}, \\ \epsilon^2 &= \frac{k_3 k_8}{k_1 k_5}, & \xi &= \frac{k_4}{\sqrt{2k_2 k_8}}, & \delta &= \frac{k_6}{k_8}. \end{aligned} \tag{4}$$

The reasoning for the choice of subscript for the phase space variables will become apparent from the blow-up in Section 3.

| | μ | α | ϵ_b | ϵ^2 | ξ | δ | κ |
|--------------|-------|----------|--------------|--------------|-------|---------------------|----------|
| $k_1 = 0.16$ | 0.97 | 0.15 | 0.0095 | 0.033 | 0.98 | $1.2 \cdot 10^{-5}$ | 3.93 |
| $k_1 = 0.35$ | 0.97 | 0.32 | 0.045 | 0.015 | 0.98 | $1.2 \cdot 10^{-5}$ | 3.93 |
| $k_1 = 0.41$ | 0.97 | 0.37 | 0.062 | 0.013 | 0.98 | $1.2 \cdot 10^{-5}$ | 3.93 |

Table 2: Standard parameter values for the Olsen model (3) obtained via the transformation (4) from Table 1; only approximate values for two significant digits are given.

The original parameter values by Olsen from Table 1 are converted into the new parameters in Table 2. The transformation already makes the multiple time scale structure of the Olsen model more visible. It is very important to note from Table 2 that varying k_1 changes the orders of magnitude for the small parameters ϵ_b and ϵ as well as their relative size. This effect has to be used in the mathematical analysis to distinguish different regimes; see also Section 8.

The general strategy to understand the Olsen model, as shown for other multiple time scale systems e.g. in [28], will be to first resolve the fastest dynamics of (3). The fastest dynamics is visible using the rescaling

$$a = a_2, \quad b = b_2, \quad x = \epsilon x_2, \quad y = \epsilon^2 y_2, \quad \tau = \epsilon^{-2} s \quad (5)$$

which, upon applying (5) to (3), yields

$$\begin{aligned} \frac{da}{d\tau} &= \epsilon^2(\mu - \alpha a) - aby, \\ \frac{db}{d\tau} &= \epsilon(\epsilon_b \epsilon - \epsilon_b bx) - \epsilon_b aby, \\ \epsilon \frac{dx}{d\tau} &= -x^2 + \epsilon(b - \xi)x + 3aby + \epsilon^2 \delta, \\ \frac{dy}{d\tau} &= \kappa(x^2 - y - aby). \end{aligned} \quad (6)$$

The two systems (3) and (6) are going to be two main components of our analysis. Notice that different regimes can exist depending upon the (relative) size of the three natural small parameters ϵ , ϵ_b and δ . In fact, just viewing (6) on a formal level, all the different fast-slow possibilities for a four-dimensional system occur in Olsen model:

- for (3), $\epsilon^2 \rightarrow 0$ yields two fast and two slow variables,
- for (3), $\epsilon^2 \neq 0$ and $\epsilon_b \rightarrow 0$ yields three fast variables and one slow variable,
- for (6), $\epsilon \rightarrow 0$ and $\epsilon_b \neq 0$ yields one fast variable and three slow variables.

All the different regimes are relevant for the asymptotic analysis of oscillatory dynamics in the Olsen model. In particular, three major regimes are relevant

$$\epsilon_b \ll \epsilon^2, \quad \epsilon_b \approx \epsilon^2, \quad \epsilon_b \gg \epsilon^2,$$

which roughly correspond to the three cases $k_1 = 0.16$, $k_1 = 0.35$ and $k_1 = 0.41$ from Table 2. In this paper, we focus on regular oscillations as displayed in Figure 1(c); but see Section 8 for the other two regimes. For the analysis in Sections 3-7 we assume that

$$0 < \epsilon^2 \ll \epsilon_b, \quad (7)$$

where ϵ_b will be regarded as a fixed parameter and singular limits are only considered with respect to a single time scale separation parameter $0 < \epsilon \ll 1$. Then observe that (6) has a critical manifold for the singular limit $\epsilon = 0$ given by

$$\mathcal{C}_0 = \left\{ (x, y, a, b) \in \mathbb{R}^4 : \frac{x^2}{3ab} = y \right\}. \quad (8)$$

For all the oscillatory patterns we are interested in, the conditions $a > a^* \geq 0$ and $b > b^* \geq 0$ hold for suitable bounded constants a^* and b^* . This implies that \mathcal{C}_0 is a well-defined critical manifold in the region

$$\mathcal{D} := \{(a, b, x, y) \in \mathbb{R}^4 : a > a^*, b > b^*, x \geq 0, y \geq 0\}.$$

We are going to assume from now on that all calculations are carried out within \mathcal{D} . Hence, all sets in the following are understood as intersections with \mathcal{D} . Then \mathcal{C}_0 is normally hyperbolic attracting for (6) when $x > 0$. Indeed, consider the fastest component of the vector field on the time scale $\tilde{\tau} := \tau/\epsilon$ given by

$$F(a, b, x, y; \epsilon) := -x^2 + \epsilon(b - \xi)x + 3aby + \epsilon^2\delta.$$

Then the attraction for $x > 0$ follows since we just have

$$\left[\frac{\partial F}{\partial x}(a, b, x, y; 0) \right] \Big|_{\{x>0\}} = -2x|_{\{x>0\}} < 0.$$

The results of Fenichel [21] and Tikhonov [71] (see Appendix A) immediately imply the next result.

Proposition 2.1. *Consider a trajectory*

$$\gamma(\tau) = (a(\tau), b(\tau), x(\tau), y(\tau)), \quad \tau \in [0, T], \quad T > 0$$

of (6) with initial value $a(0), b(0), x(0), y(0) \in \mathcal{D}$ such that

$$a(0), b(0), x(0), y(0) > 0 \quad \text{and} \quad a(0), b(0), x(0), y(0) = \mathcal{O}(1) \text{ as } \epsilon \rightarrow 0.$$

Assume $0 < \epsilon \ll 1$ is sufficiently small and all other parameters are fixed and positive. Then $\gamma(\tau)$ is $\mathcal{O}(e^{-K/\epsilon})$ -close to the slow manifold \mathcal{C}_ϵ after a finite time $\tau^ \in [0, T]$.*

Proposition (2.1) essentially describes the fastest initial dynamics for most initial conditions. Trajectories are just attracted towards \mathcal{C}_0 . The three-dimensional flow on \mathcal{C}_0 in the

normally hyperbolic regime is considered in Section 5. It will be shown that trajectories may also reach a neighbourhood of the set

$$\mathcal{L}_0 := \{(a, b, x, y) \in \mathcal{D} : x = 0 = y\} \subset \mathcal{C}_0.$$

We observe that \mathcal{L}_0 is a submanifold of non-degenerate fold points since

$$F(a, b, 0, 0; 0) = 0, \quad \frac{\partial F}{\partial x}(a, b, 0, 0; 0) = 0, \quad \frac{\partial^2 F}{\partial x^2}(a, b, 0, 0; 0) = 0, \quad \frac{\partial F}{\partial y}(a, b, 0, 0; 0) \neq 0,$$

where we used that $a > a^* > 0$, $b > b^* > 0$ in \mathcal{D} for the y -derivative. The fold manifold \mathcal{L}_0 is not normally hyperbolic and has to be desingularized. The analysis of the fold region is contained in Sections 3-4.

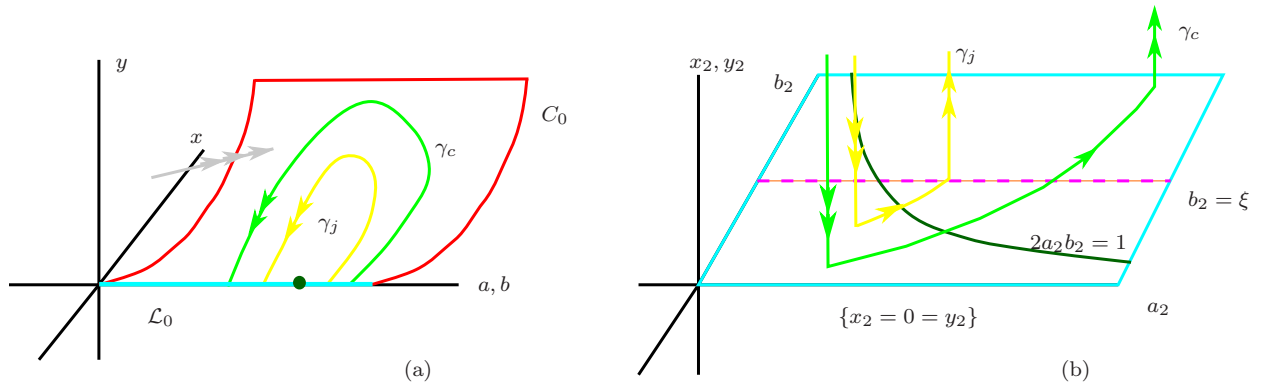


Figure 2: Sketch of the basic geometry for the two types of non-classical relaxation oscillations inside the region \mathcal{D} . (a) Phase space for the system (6) which captures the large fast loops. The critical manifold C_0 (red), two segments of the candidate orbits γ_c (green) and γ_j (yellow), the fold manifold \mathcal{L}_0 (cyan), the submanifold $\{2ab = 1, x = 0 = y\}$ (dark-green dot) and the “super-fast” attracting dynamics (grey triple arrow) are shown. (b) Phase space for (6) which focuses on the slow drift near \mathcal{L}_0 (cyan). We show segments of the two candidate orbits γ_c (green), γ_j (yellow), the exchange-of-stability line $\{b_2 = \xi\}$ (magenta) and the submanifold $\{2a_2b_2 = 1, x_2 = 0 = y_2\}$ (dark-green curve). For a description of the dynamics please refer to the text in Section 2.

Before we proceed to state our main result, we shall motivate the geometric construction briefly on a non-rigorous level as outlined in Figure 2. For the following discussion, we refer to objects in singular limits, which we have to perturb later on. We start with system (6) and apply Proposition 2.1 to understand the “super-fast” dynamics on the time scale $\tilde{\tau} := \tau/\epsilon$. Trajectories get attracted to C_0 . On C_0 , (6) yields a three-dimensional vector field on the time scale τ

$$\begin{aligned} \frac{da}{d\tau} &= -aby, \\ \frac{db}{d\tau} &= -\epsilon_b aby, \\ \frac{dy}{d\tau} &= \kappa(2ab - 1)y, \end{aligned} \tag{9}$$

where we have just used $x^2 = 3aby$ and $\epsilon = 0$. It turns out that (9) can be solved explicitly, albeit with relatively inconvenient formulas. Although (9) is formally a “slow subsystem”

we shall refer to it as the fast dynamics as we shall discover another (even “slower”) system inside \mathcal{L}_0 . After some calculations, the solutions of (9) turn out to be arcs as indicated by Figure 2(a) connecting two points on \mathcal{L}_0 . Furthermore, one can view these solutions as jumps over a submanifold $\{2ab = 1\}$, which we indicated as a dot in Figure 2(a). Since these arcs start and end in the singular locus of fold points \mathcal{L}_0 we proceed to system (3), which is a “zoom” of (6) near \mathcal{L}_0 . One notices that for (3), upon taking $\epsilon = 0 = \delta$, one part of the two-dimensional critical manifold is given by $\{x_2 = 0 = y_2\}$. The results from Section 3 are going to yield that $\{x_2 = 0 = y_2\}$ is attracting for $b_2 < \xi$ and repelling for $b_2 > \xi$; see also Figure 2(b). We denote these attracting and repelling parts by $\mathcal{S}_{2,0}^{a-}$ and $\mathcal{S}_{2,0}^{r+}$. Let us follow candidate trajectories which get attracted to $\mathcal{S}_{2,0}^{a-}$, such as γ_c or γ_j shown in Figure 2(b). Once $\gamma_{c,j}$ reach $\mathcal{S}_{2,0}^{a-}$ their dynamics is governed by taking $\epsilon = 0$ in (6) i.e.

$$\begin{aligned}\frac{da_2}{ds} &= \mu - \alpha a_2, \\ \frac{db_2}{ds} &= \epsilon_b,\end{aligned}\tag{10}$$

which has very simple explicit solution formulas. However, the fast direction stability changes at $b_2 = \xi$. It can be proven that for $\delta = 0$, we may view $\{b_2 = \xi\}$ as a submanifold of trans-critical singularities where maximal delay occurs so that γ_c is a canard trajectory traveling for a considerable time onto $\mathcal{S}_{2,0}^{r+}$ before it eventually jumps; see Figure 2(b). However, if $\delta > 0$ is positive and not exponentially small with respect to ϵ , then we are in the case γ_j where the candidate orbit jumps near $\{b_2 = \xi\}$. In both cases, $\gamma_{c,j}$ are then in a fast regime away after their departure from $\mathcal{S}_{2,0}^{r+}$, which allows us to connect them back from Figure 2(b) to 2(a). Taking a global view, it is then possible to construct two types of candidate periodic orbits γ_j and γ_c which can then be shown to perturb to periodic orbits for $0 < \epsilon \ll 1$. The precise statement is as follows:

Theorem 2.2. *There exists a family of open sets $(\mu_1(\epsilon), \mu_2(\epsilon))$ for some $\mu_i > 0$ with $i = 1, 2$ and $\epsilon_0 > 0$ sufficiently small such that the Olsen model (6) for $\mu \in (\mu_1(\epsilon), \mu_2(\epsilon))$ with $\epsilon \in (0, \epsilon_0]$ and otherwise standard parameter values from Table 2 with $k_1 = 0.41$ has a family of periodic orbits ψ_ϵ in the following two cases:*

1. **Canard case:** *Suppose $\delta = \mathcal{O}(\epsilon^2 e^{-K_1/\epsilon^2})$ and $K_1 > 0$ is some fixed constant independent of ϵ . Then ψ_ϵ has a canard segment which is $\mathcal{O}(\epsilon^2)$ -close to a repelling part of $\{x_2 = 0 = y_2\}$ for a time $s^* = \mathcal{O}(1)$, $s^* > 0$ as $\epsilon \rightarrow 0$.*
2. **Jump case:** *Suppose $\delta = K_2 \epsilon^2$, $K_2 > 0$ and K_2 is fixed as $\epsilon \rightarrow 0$. Then ψ_ϵ does not have a canard segment and leaves \mathcal{L}_0 in an ϵ -dependent neighbourhood $\mathcal{N}(\epsilon)$ of $\{b_2 = \xi\}$ such that $d_H(\mathcal{N}(\epsilon), \{b_2 = \xi\}) \rightarrow 0$ as $\epsilon \rightarrow 0$.*

In both cases, ψ_0 is a candidate orbit with a slow segment in \mathcal{L}_0 and a fast segment in \mathcal{C}_0 and $d_H(\psi_\epsilon, \psi_0) \rightarrow 0$ as $\epsilon \rightarrow 0$. In both cases, ψ_ϵ is locally asymptotically stable.

The situation is also illustrated in Figure 2. Heuristically, in view of the discussion preceding Theorem 2.2, we may concisely summarize the result as follows (see Figure 2):

1. If δ is zero or exponentially small then we have a periodic orbit converging to a candidate orbit with a canard segment i.e. $d_H(\psi_\epsilon, \gamma_c) \rightarrow 0$ as $\epsilon \rightarrow 0$.

2. If δ scales like ϵ^2 then we have a periodic orbit converging to a candidate orbit, without a canard segment and jumping near a (transcritical) singularity, i.e. $d_H(\psi_\epsilon, \gamma_j) \rightarrow 0$ as $\epsilon \rightarrow 0$.

Of course, one may also aim to consider other situations. For example, if $\delta \gg \epsilon^2$ then our analysis does not apply but this case does not occur in the original parameter sets used by Olsen, so we shall not discuss it here. However, there is an interesting case which occurs when

$$0 < \epsilon^2 e^{-K/\epsilon} \ll \delta \ll \epsilon^2 \ll 1. \quad (11)$$

In this case, the family periodic orbits with a canard segment deforms smoothly into the periodic family of the jump case as δ increases. In fact, this is precisely the case which occurs for the classical Olsen parameter values from Table 2 since $\epsilon^2 = 1.5 \cdot 10^{-2}$ and $\delta = 1.2 \cdot 10^{-5}$. As usual when applying GSPT, it is helpful to focus on the two limiting cases to describe an intermediate asymptotic regime. Desroches et al. [15] computed numerical bifurcation diagrams for the Olsen model and observed that “the bifurcation structure does not change in an essential way” [15] when the same types of diagrams were computed for $\delta = 0$ and $\delta = 1.2 \cdot 10^{-5}$. In fact, our result shows that there will be a substantial deformation of orbits in the system depending upon δ . However, this is no contradiction as the bifurcation diagram may not change significantly, when plotted in parameter space only, as there is a family of periodic orbits, whether $\delta = 0$ or $\delta = 1.2 \cdot 10^{-5}$.

The orbit ψ_ϵ from Theorem 2.2 has relaxation-type properties as it consists of alternating fast and slow segments but it is not a classical relaxation oscillation generated by a cubic critical manifold mechanism [73, 24]. Hence we use the term non-classical relaxation oscillation. In Sections 3-7 we proceed to provide a proof of Theorem 2.2.

3 The Main Blow-Up

We start with the analysis near the fold locus \mathcal{L}_0 which will require a blow-up; see Appendix B as well as [18, 47] for background on geometric desingularization via the blow-up method. Coefficients to desingularize (6) are suggested by the scaling (5). Let

$$\bar{\mathcal{D}} := [a^*, \infty) \times [b^*, \infty) \times (\mathcal{S}^2)_0^+ \times [0, r_0]$$

for $r_0 > 0$ where $(\mathcal{S}^2)_0^+ \subset \mathbb{R}^3$ denotes the upper half of the unit sphere including the equator. Changing the time scale to $t = \tau/\epsilon$ and augmenting (6) by $\epsilon' = 0$ yields

$$\begin{aligned} a' &= \epsilon^3(\mu - \alpha a) - \epsilon aby, \\ b' &= \epsilon^2(\epsilon_b \epsilon - \epsilon_b bx) - \epsilon \epsilon_b aby, \\ x' &= -x^2 + \epsilon(b - \xi)x + 3aby + \epsilon^2 \delta, \\ y' &= \epsilon \kappa(x^2 - y - aby), \\ \epsilon' &= 0. \end{aligned} \quad (12)$$

Consider the blow-up transformation $\Phi : \bar{\mathcal{D}} \rightarrow \mathcal{D}$ defined via

$$a = \bar{a}, \quad b = \bar{b}, \quad x = \bar{r}\bar{x}, \quad y = \bar{r}^2\bar{y}, \quad \epsilon = \bar{r}\bar{\epsilon} \quad (13)$$

where $(\bar{x}, \bar{y}, \bar{\epsilon}) \in (\mathcal{S}^2)_0^+$. Φ blows up the vector field V given by (12); see also Figure 3(b). The map Φ induces a vector field \bar{V} on $\bar{\mathcal{D}}$ by pushforward $\Phi_*(\bar{V}) = V$. To analyze \bar{V} it is convenient to consider the manifold $\bar{\mathcal{D}}$ in several charts. Define the following submanifolds

$$\bar{\mathcal{D}}_{\bar{x}} := \bar{\mathcal{D}} \cap \{\bar{x} > 0\} \quad \text{and} \quad \bar{\mathcal{D}}_{\bar{\epsilon}} := \bar{\mathcal{D}} \cap \{\bar{\epsilon} > 0\}.$$

The submanifold $\bar{\mathcal{D}}_{\bar{y}}$ can also be considered but will yield the same qualitative view of the dynamics as $\bar{\mathcal{D}}_{\bar{x}}$. Hence we are not going to need it for our analysis.

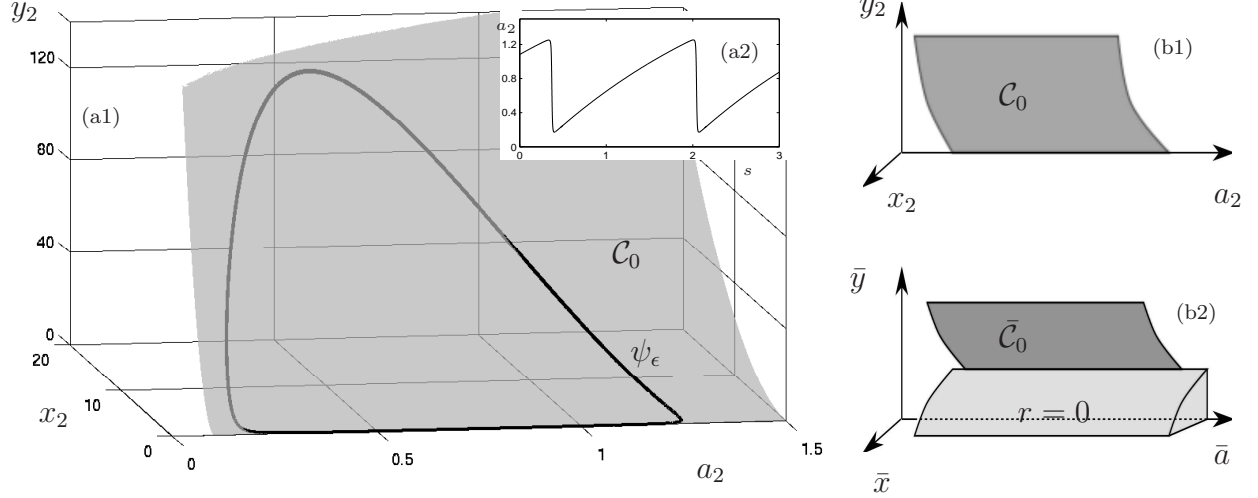


Figure 3: Illustration of the non-classical relaxation orbit ψ_ϵ , the critical manifold \mathcal{C}_0 and the blow-up. (a1) Projection into (a_2, x_2, y_2) -space of an integration of the full system (3) with standard parameter values from Table 2 and $k_1 = 0.41$. (a2) Time series for the variable a . (b1) Sketch of the situation before the blow-up with the critical manifold (dark gray). (b2) Blown-up space where the fold points have been desingularized by the transformation (13) inserting a cylinder (light gray) giving the new domain $\bar{\mathcal{D}}$.

Lemma 3.1. *The maps $\kappa_1 : \bar{\mathcal{D}}_{\bar{x}} \rightarrow \mathcal{D}$ for $(a_1, b_1, r_1, y_1, \epsilon_1) \in \bar{\mathcal{D}}_{\bar{x}}$ and $\kappa_2 : \bar{\mathcal{D}}_{\bar{\epsilon}} \rightarrow \mathcal{D}$ for $(a_2, b_2, x_2, y_2, r_2) \in \bar{\mathcal{D}}_{\bar{\epsilon}}$ given by*

$$\begin{aligned} a_1 &= \bar{a}, & b_1 &= \bar{b}, & r_1 &= \bar{r}\bar{x}, & y_1 &= \bar{x}^{-2}\bar{y}, & \epsilon_1 &= \bar{x}^{-1}\bar{\epsilon} \\ a_2 &= \bar{a}, & b_2 &= \bar{b}, & x_2 &= \bar{\epsilon}^{-1}\bar{x}, & y_2 &= \bar{\epsilon}^{-2}\bar{y}, & r_2 &= \bar{r}\bar{\epsilon} \end{aligned}$$

define charts for $\bar{\mathcal{D}}$ in which the blow-up Φ is, respectively, given by

$$\begin{aligned} a &= a_1, & b &= b_1, & x &= r_1, & y &= r_1^2 y_1, & \epsilon &= r_1 \epsilon_1, \\ a &= a_2, & b &= b_2, & x &= r_2 x_2, & y &= r_2^2 y_2, & \epsilon &= r_2. \end{aligned} \tag{14}$$

Proof. Consider κ_1 then $r_1 = \bar{r}\bar{x}$ but since for Φ we have $\bar{r}\bar{x} = x$ it follows that $x = r_1$. Furthermore

$$r_1^2 y_1 = r_1^2 \bar{x}^{-2} \bar{y} = x^2 \bar{x}^{-2} \bar{y} = \bar{r}^2 \bar{x}^2 \bar{x}^{-2} \bar{y} = \bar{r}^2 \bar{y} = y.$$

The calculation for ϵ and the second chart κ_2 are similar. \square

Observe that the blow-ups (14) in the charts κ_1 and κ_2 are essentially defined by the conditions $\bar{x} = 1$ and $\bar{\epsilon} = 1$.

Lemma 3.2. *The coordinate change κ_{12} from the first to the second chart and its inverse are*

$$\begin{aligned} a_2 &= a_1, & b_2 &= b_1, & x_2 &= \epsilon_1^{-1}, & y_2 &= y_1 \epsilon_1^{-2}, & r_2 &= r_1 \epsilon_1 \\ a_1 &= a_2, & b_1 &= b_2, & r_1 &= r_2 x_2, & y_1 &= y_2 x_2^{-2}, & \epsilon_1 &= x_2^{-1}. \end{aligned} \quad (15)$$

With the charts available we can calculate the blown-up vector fields in each chart.

Lemma 3.3. *In the chart κ_1 the desingularized blown-up vector field is given by*

$$\begin{aligned} a'_1 &= \epsilon_1 r_1^2 [\epsilon_1^2 (\mu - \alpha a_1) - a_1 b_1 y_1], \\ b'_1 &= \epsilon_1 r_1^2 \epsilon_b [\epsilon_1^2 - \epsilon_1 b_1 - a_1 b_1 y_1], \\ r'_1 &= r_1 [-1 + \epsilon_1 (b_1 - \xi) + 3a_1 b_1 y_1 + \epsilon_1^2 \delta], \\ y'_1 &= \kappa \epsilon_1 (1 - y_1 (1 + a_1 b_1)) - 2y_1 (-1 + \epsilon_1 (b_1 - \xi) + 3a_1 b_1 y_1 + \epsilon_1^2 \delta), \\ \epsilon'_1 &= -\epsilon_1 [-1 + \epsilon_1 (b_1 - \xi) + 3a_1 b_1 y_1 + \epsilon_1^2 \delta]. \end{aligned} \quad (16)$$

Proof. The equations for a_1 , b_1 and r_1 are easy to obtain. For y_1 we calculate

$$y' = 2r_1 r'_1 y_1 + r_1^2 y'_1 \quad \Rightarrow \quad y'_1 = \frac{y' - 2r_1 y_1 r'_1}{r_1^2}.$$

Substituting y' from (12) and using (14) gives y'_1 . The calculation for ϵ'_1 is easier since $\epsilon' = 0$. All equations derived in this way have a multiplicative pre-factor of r_1 , which can be removed by a time rescaling which yields the desingularized vector field (16). \square

In the chart κ_2 the blow-up (14) reduces to the rescaling

$$a = a_2, \quad b = b_2, \quad x = \epsilon x_2, \quad y = \epsilon^2 y_2. \quad (17)$$

Lemma 3.4. *In the chart κ_2 the blown-up vector field is given by*

$$\begin{aligned} \frac{da_2}{ds} &= \mu - \alpha a_2 - a_2 b_2 y_2, \\ \frac{db_2}{ds} &= \epsilon_b (1 - b_2 x_2 - a_2 b_2 y_2), \\ \epsilon^2 \frac{dx_2}{ds} &= 3a_2 b_2 y_2 - x_2^2 + (b_2 - \xi) x_2 + \delta, \\ \epsilon^2 \frac{dy_2}{ds} &= \kappa (x_2^2 - y_2 - a_2 b_2 y_2). \end{aligned} \quad (18)$$

where the time scale is $s = \epsilon^2 \tau$.

Hence, the re-scaled version (3) of the Olsen model we derived from Olsen's original equations (2) just resolves the dynamics well on one scale in a certain region of phase space. When the blow-up reduces to a re-scaling as in κ_2 , then one also refers to the corresponding chart as the classical chart [69]. The chart κ_1 describes the regime where trajectories approach the submanifold of folds \mathcal{L}_0 from the three-dimensional slow flow discussed in Section 5. Hence we are going to discuss κ_1 first.

3.1 First Chart

The approach towards and departure from a submanifold

$$[a^*, \infty) \times [b^*, \infty) \times (\mathcal{S}^2)_0^+ \times \{\bar{r} = 0\} \cap \{\bar{x} > 0\}$$

consisting of an (\bar{a}, \bar{b}) -dependent family of spheres can be studied best in the chart κ_1 . In particular, we study the ODEs (16) from Lemma 3.3 in this section. The case $\epsilon_1 = 0$ corresponds to the equator of the spheres.

Lemma 3.5. *There exists a dimension two foliation with leaves*

$$\{\epsilon_1 = 0, a_1 = a_1^*, b_1 = b_1^*\} \quad (19)$$

with constants a_1^*, b_1^* for (16). The vector field in the invariant submanifolds (19) is given by

$$\begin{aligned} r_1' &= r_1 (3a_1^* b_1^* y_1 - 1), \\ y_1' &= -2y_1 (3a_1^* b_1^* y_1 - 1). \end{aligned} \quad (20)$$

The proof of Lemma 3.5 follows by direct substitution of the algebraic conditions defining (19) into (16). The planar system (20) can be analyzed directly using standard phase plane methods and linearization. Recall that we are only interested in the case $y_1 \geq 0$ and $r_1 \geq 0$.

Lemma 3.6. *The ODE (20) has (see also Figure 4)*

- a saddle equilibrium at $(r_1, y_1) = (0, 0)$ with eigenvalues $\lambda_1 = -1$, $\lambda_2 = 2$ and eigendirections $v_1 = (1, 0)^T$, $v_2 = (0, 1)^T$;
- a line of degenerate equilibrium points $\{y_1 = 1/(3a_1^* b_1^*)\}$ which is attracting in the v_2 direction.

The line $\{y_1 = 1/(3a_1^* b_1^*)\}$ corresponds to the attracting critical manifold \mathcal{C}_0 defined in (8).

Proof. The calculations to find the equilibria and their stability are straightforward. Regarding the last statement about \mathcal{C}_0 , observe that Lemma 3.1 implies $x^2 = r_1^2$ and $y = r_1^2 y_1$ so

$$\Phi \circ \kappa_1^{-1}(\{y_1 = 1/(3a_1 b_1)\}) = \Phi \circ \kappa_1^{-1}(\{y_1 r_1^2 = r_1^2/(3a_1 b_1)\}) = \{y = x^2/(3ab)\}. \quad \square$$

There is a natural second family of invariant subspaces for (16) for the case $r_1 = 0$ (i.e. “on the sphere”) which yields a more complicated family of flows. To analyze this case, we shall assume that

$$\delta = \delta(\epsilon) \quad \text{and} \quad \delta(0) = 0. \quad (21)$$

Note that (21) holds for the canard case and the jump case in Theorem 2.2.

Lemma 3.7. *Suppose (21) holds. Then there exists a dimension two foliation with leaves*

$$\{r_1 = 0, a_1 = a_1^*, b_1 = b_1^*\} \quad (22)$$

with constants a_1^*, b_1^* for (16). The vector field in the invariant submanifolds (22) is given by

$$\begin{aligned} y_1' &= \kappa \epsilon_1 (1 - y_1 (1 + a_1^* b_1^*)) - 2y_1 (-1 + \epsilon_1 (b_1^* - \xi) + 3a_1^* b_1^* y_1), \\ \epsilon_1' &= -\epsilon_1 [-1 + \epsilon_1 (b_1^* - \xi) + 3a_1^* b_1^* y_1]. \end{aligned} \quad (23)$$

The proof of Lemma 3.5 follows by direct substitution of the algebraic conditions defining (22) into (16) and using $\delta(0) = 0$. For the analysis of (23) we start with the case

$$|\xi - b_1^*| \geq K > 0 \quad \text{for a fixed constant } K \text{ independent of } \epsilon. \quad (24)$$

The situation near $|\xi - b_1^*| = 0$ is different and will be covered at the end of this section. If (24) holds, there are three equilibrium points

$$\begin{aligned} (y_1, \epsilon_1) &= (0, 0) =: p_1, \\ (y_1, \epsilon_1) &= \left(\frac{1}{3a_1^*b_1^*}, 0 \right) =: p_2, \\ (y_1, \epsilon_1) &= \left(\frac{1}{1+a_1^*b_1^*}, \frac{1-2a_1^*b_1^*}{(1+a_1^*b_1^*)(b_1^*-\xi)} \right) =: p_3. \end{aligned} \quad (25)$$

To determine the stability of the eigenvalues we calculate the linearization for (23) with Jacobian(s)

$$\begin{aligned} A_{1j} &:= D_{y_1, \epsilon_1} \begin{pmatrix} y_1' \\ \epsilon_1' \end{pmatrix} \Big|_{p_j} = \\ &= \begin{pmatrix} 2 - a_1^*b_1^*(12y_1 + \epsilon_1\kappa) - \epsilon_1(2b_1^* + \kappa - 2\xi) & \kappa - y_1(\kappa + b_1^*(2 + a_1^*\kappa) - 2\xi) \\ -3a_1^*b_1^*\epsilon_1 & 1 - 3a_1^*b_1^*y_1 - 2b_1^*\epsilon_1 + 2\epsilon_1\xi \end{pmatrix} \Big|_{p_j} \end{aligned} \quad (26)$$

The next result summarizes the relevant stability information for the three equilibrium points.

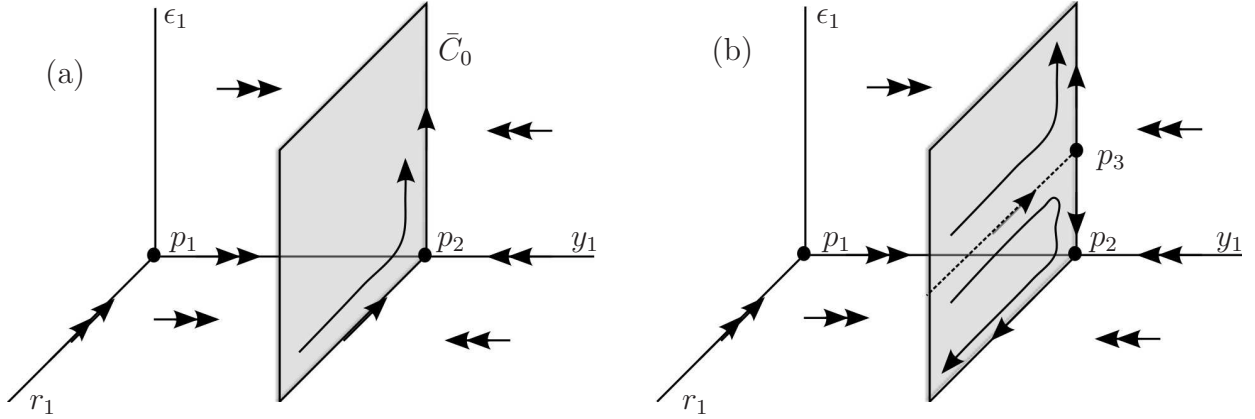


Figure 4: Sketch of the flows for the chart κ_1 for (16). The variables $a_1 = a_1^*$ and $b_1 = b_1^*$ are fixed and the case $b_1^* < \xi$ is shown. The gray surface indicates the blow-up of the critical manifold C_0 which corresponds to the center manifold \mathcal{M}_1 . Double arrows indicate strong attraction or repulsion and single arrows indicate a center flow. (a) $2a_1^*b_1^* < 1$: Due to the center flow on \mathcal{M}_1 trajectories approach the sphere and flow upwards near the saddle p_2 . (b) $2a_1^*b_1^* > 1$: The additional equilibrium p_3 may prevent the flow up the sphere.

Lemma 3.8. *Suppose (24) holds. The equilibria of (23) have the following types*

- p_1 is an unstable node with eigenvalues 1 and 2,

- p_2 is center-stable with eigenvalues -2κ and 0. The stable manifold associated to the eigenvalue -2κ is given by

$$W^s(p_2) = \{(y_1, \epsilon_1) \in \mathbb{R}^2 : \epsilon_1 = 0, y_1 > 0\}.$$

Furthermore, $p_3 \notin \bar{\mathcal{D}}_\epsilon$ for $(\xi - b_1^*)(2a_1^*b_1^* - 1) < 0$, $p_3 \in \bar{\mathcal{D}}_\epsilon$ for $(\xi - b_1^*)(2a_1^*b_1^* - 1) > 0$ and $p_3 = p_2$ when $2a_1^*b_1^* = 1$. If $p_3 \in \bar{\mathcal{D}}_\epsilon$ then

- p_3 is a saddle for $b_1^* < \xi$,
- p_3 is a sink for $b_1^* > \xi$.

Proof. The stability results for p_1 and p_2 follow immediately by looking at the 2×2 -matrices A_{11} and A_{12} from (26). The stable manifold result for p_2 follows from the local information at p_2 and the invariance of the $\{\epsilon_1 = 0\}$ -subspace of (23). Looking at the sign of the ϵ_1 -component of p_3 implies when p_3 is visible in the domain $\bar{\mathcal{D}}_\epsilon$. For the stability, we consider $A_{13} \in \mathbb{R}^{2 \times 2}$ from (26). If $b_1^* < \xi$ then p_3 is a saddle since

$$\det(A_{13}) = \frac{(1 - 2a_1^*b_1^*)^2\kappa}{(1 + a_1^*b_1^*)(b_1^* - \xi)} < 0.$$

Another direct calculation yields, using $(\xi - b_1^*)(2a_1^*b_1^* - 1) > 0$, that

$$\text{trace}(A_{13}) = -4 + \frac{3}{1 + a_1^*b_1^*} + \frac{(2a_1^*b_1^* - 1)\kappa}{b_1^* - \xi} < -4 + \frac{3}{1 + a_1^*b_1^*} < 0$$

so that for $b_1^* > \xi$ the equilibrium p_3 is a sink. \square

The equilibrium point p_3 passes from the lower-half of the sphere $\epsilon_1 < 0$ to the upper half $\epsilon_1 > 0$ on the curve $2a_1^*b_1^* = 1$. This implies that the flow on the upper half-sphere has two different regimes. Furthermore, the type of the equilibria may change based upon the two sub-cases given by $b_1^* < \xi$ and $b_1^* > \xi$. This shows the necessity to consider the incoming flow towards the fold submanifold very carefully as the variables (a, b) act as additional parameters for the invariant foliations in the chart κ_1 .

Since p_2 always exists as an equilibrium point and has one center direction, it is necessary to calculate the center manifold. In particular, we return to the system

$$\begin{aligned} r_1' &= r_1 [-1 + \epsilon_1(b_1^* - \xi) + 3a_1^*b_1^*y_1], \\ y_1' &= \kappa\epsilon_1(1 - y_1(1 + a_1^*b_1^*)) - 2y_1(-1 + \epsilon_1(b_1^* - \xi) + 3a_1^*b_1^*y_1), \\ \epsilon_1' &= -\epsilon_1[-1 + \epsilon_1(b_1^* - \xi) + 3a_1^*b_1^*y_1]. \end{aligned} \quad (27)$$

Proposition 3.9. *The center manifold \mathcal{M}_1 for (27) at the equilibrium p_2 is given as the graph of*

$$y_1 = \frac{1}{3a_1^*b_1^*} + \epsilon_1 \frac{2(\xi - b_1^*) + \kappa(2a_1^*b_1^* - 1)}{6a_1^*b_1^*} + c_{22}\epsilon_1^2 + \mathcal{O}(\epsilon_1^3, \epsilon_1^2 r_1, \epsilon_1 r_1^2, r_1^3) \quad (28)$$

where

$$c_{22} = \frac{\kappa(1 + 4a_1^*b_1^*)}{24a_1^*b_1^*}(2(b_1^* - \xi) + \kappa(1 - 2a_1^*b_1^*)).$$

The flow on \mathcal{M}_1 is

$$\begin{aligned} r_1' &= r_1 \left[\frac{\kappa(2a_1^*b_1^*-1)}{2} \epsilon_1 + 3a_1^*b_1^*c_{22}\epsilon_1^2 + \mathcal{O}(\epsilon_1^3, \epsilon_1^2r_1, \epsilon_1r_1^2, r_1^3) \right], \\ \epsilon_1' &= -\epsilon_1 \left[\frac{\kappa(2a_1^*b_1^*-1)}{2} \epsilon_1 + 3a_1^*b_1^*c_{22}\epsilon_1^2 + \mathcal{O}(\epsilon_1^3, \epsilon_1^2r_1, \epsilon_1r_1^2, r_1^3) \right]. \end{aligned} \quad (29)$$

For $b_1^* < \xi$ there are two qualitative cases for the flow (29) near the center manifold as shown in Figure 4. For $b_1^* > \xi$ the center flow in 4(a) is directed away from the sphere while the equilibrium p_3 becomes a sink in Figure 4(b).

Remark: Note that the center flow is very degenerate when $2a_1^*b_1^* = 1$ and $b_1^* = \xi$. This corresponds to the case when the initial conditions in the chart κ_1 lie exactly on the degenerate singularity $(a, b) = (1/(2\xi), \xi)$. It will be shown in Section 5 that this case will not occur due to the form of the slow flow on \mathcal{C}_0 for the periodic orbits we consider in this paper; see Figure 2.

Proof. (of Proposition 3.9) The center manifold calculation is contained in Appendix C which yields (28) and consequently also (29). The results in Figure 4 follow from Lemma 3.6, Lemma 3.8 and phase plane analysis of (29) for the two cases $2a_1^*b_1^* > 1$ and $2a_1^*b_1^* < 1$. More precisely, desingularizing (29) by rescaling time with $1/\epsilon_1$ we note that $(r_1, \epsilon_1) = (0, 0) =: 0$ is saddle for (29). If $2a_1^*b_1^* < 1$ then the stable and unstable eigenspaces are locally given by $E^s(0) = \{\epsilon_1 = 0\}$ and $E^u(0) = \{r_1 = 0\}$. The local directions are reversed for $2a_1^*b_1^* > 1$ so that $E^u(0) = \{\epsilon_1 = 0\}$ and $E^s(0) = \{r_1 = 0\}$. \square

Using Proposition 2.1, the correspondence of \mathcal{C}_0 and \mathcal{M}_1 via Lemma 3.6, the exponential attraction of \mathcal{M}_1 in the y_1 -direction and the description of the flow (29) in Proposition 3.9, it follows that, depending on the invariant foliation determined by the coordinates (a_1^*, b_1^*) , several cases can occur.

Proposition 3.10. *Suppose (24) holds, then four cases can occur*

- (C1) *If $2a_1^*b_1^* < 1$, $b_1^* < \xi$ then orbits approach $\bar{\mathcal{D}} \cap \{\bar{r} = 0\}$ and flow up the family of spheres into the chart κ_2 .*
- (C2) *If $2a_1^*b_1^* < 1$, $b_1^* > \xi$ then orbits approach $\bar{\mathcal{D}} \cap \{\bar{r} = 0\}$ and flow up the family of spheres into the chart κ_2 towards the sink p_3 .*
- (C3) *If $2a_1^*b_1^* > 1$ and $b_1^* < \xi$ then orbits may either approach $\bar{\mathcal{D}} \cap \{\bar{r} = 0\}$ and flow up the family of spheres into the chart κ_2 , or turn around and continue in the slow flow on \mathcal{C}_0 . This case depends upon the initial condition.*
- (C4) *If $2a_1^*b_1^* > 1$ and $b_1^* > \xi$ then orbits flow away from $\bar{\mathcal{D}} \cap \{\bar{r} = 0\}$.*

For this paper, two of the cases from Proposition 3.10 are relevant. For the canard and the jump case in Theorem 2.2 we are going to need (C1) to track orbits from κ_1 to κ_2 when they enter a neighbourhood of \mathcal{L}_0 . For the canard case, we need (C4) to track orbits from κ_2 to κ_1 when they leave a neighbourhood of \mathcal{L}_0 ; see also Figure 2. Note that the points a_1^*, b_1^* are always the values of the (a, b) -coordinates once a vicinity of the center manifold \mathcal{M}_1 has been reached. Although we shall not need (C2)-(C3) here, we record them for future work; see also Section 8.

It remains to investigate the case $b_1^* = \xi$ which will be relevant for the departure phase for the jump case in Theorem 2.2. We shall only consider the following case

$$b_1^* = \xi, \quad 2a_1^*b_1^* > 1, \quad a_1^* - \frac{1}{2\xi} = K > 0 \quad \text{for a fixed constant } K \text{ independent of } \epsilon. \quad (30)$$

This means that we only track orbits transitioning between κ_2 and κ_1 away from the degenerate singularity $(a, b) = (1/(2\xi), \xi)$ and above the curve $\{2ab = 1\}$; see Figure 2(b). Under the assumption (30) the system (23) reduces to

$$\begin{aligned} y_1' &= \kappa\epsilon_1(1 - y_1(1 + a_1^*\xi)) - 2y_1(-1 + 3a_1^*\xi y_1), \\ \epsilon_1' &= -\epsilon_1[-1 + 3a_1^*\xi y_1]. \end{aligned} \quad (31)$$

It is easy to check that (31) only has the two equilibrium points

$$\begin{aligned} (y_1, \epsilon_1) &= (0, 0) =: p_1, \\ (y_1, \epsilon_1) &= \left(\frac{1}{3a_1^*b_1^*}, 0\right) =: p_2, \end{aligned} \quad (32)$$

where it is natural to use the same notation as in (25). The next result is easy to check by following the same calculations as above using the matrices $A_{11}, A_{12} \in \mathbb{R}^{2 \times 2}$ for $b_1^* = \xi$.

Lemma 3.11. *Suppose (30) holds. The equilibria of (31) are given by (32). p_1 is an unstable node with eigenvalues 1 and 2. p_2 is center-stable with eigenvalues -2κ and 0. The stable manifold associated to the eigenvalue -2κ is given by $W^s(p_2) = \{\epsilon_1 = 0, y_1 > 0\}$. Furthermore, the center manifold reduction from Proposition 3.9 is still valid.*

Corollary 3.12. *Suppose (30) holds. Then, the case (C4) from Proposition (3.10) applies to orbits transitioning from κ_2 to κ_1 .*

Proof. By Lemma 3.11 we may focus on the dynamics near p_2 and consider the center manifold reduction (29). Since $2a_1^*b_1^* > 1$ holds by (30), the result follows. \square

3.2 Second Chart

In the last section, we have controlled the flow arriving from \mathcal{C}_0 near \mathcal{L}_0 and the situation when orbits leave the vicinity of \mathcal{L}_0 towards \mathcal{C}_0 . It remains to analyze the dynamics in the chart κ_2 which describes the slow dynamics near \mathcal{L}_0 . The analysis in this section focuses on the system (18) from Lemma 3.4 which we repeat here for convenience

$$\begin{aligned} \frac{da_2}{ds} &= \mu - \alpha a_2 - a_2 b_2 y_2, \\ \frac{db_2}{ds} &= \epsilon_b(1 - b_2 x_2 - a_2 b_2 y_2), \\ \epsilon^2 \frac{dx_2}{ds} &= 3a_2 b_2 y_2 - x_2^2 + (b_2 - \xi)x_2 + \delta, \\ \epsilon^2 \frac{dy_2}{ds} &= \kappa(x_2^2 - y_2 - a_2 b_2 y_2). \end{aligned} \quad (33)$$

We are not going to make the restriction yet that $\delta = \delta(\epsilon)$ with $\delta(0) = 0$ to cover a more general case and view δ just as a parameter. Then the critical manifold of (33) is given by

$$\mathcal{C}_{2,0} := \left\{ (a_2, b_2, x_2, y_2) \in \bar{\mathcal{D}} : a_2 = \frac{x_2^2 + x_2(\xi - b_2) - \delta}{b_2(2x_2^2 + x_2(b_2 - \xi) + \delta)}, y_2 = \frac{2x_2^2 + x_2(b_2 - \xi) + \delta}{3} \right\}.$$

Let $\frac{(1+a_2b_2)(\xi-b_2)}{4a_2b_2-2} =: l_2^\delta(a_2, b_2, \xi)$ and define

$$\begin{aligned}\mathcal{S}_{2,0}^{r-} &:= \mathcal{C}_{2,0} \cap \{b_2 < \xi, x_2 > l_2^\delta(a_2, b_2, \xi)\}, \\ \mathcal{S}_{2,0}^{a-} &:= \mathcal{C}_{2,0} \cap \{b_2 < \xi, x_2 < l_2^\delta(a_2, b_2, \xi)\}, \\ \mathcal{S}_{2,0}^{r+} &:= \mathcal{C}_{2,0} \cap \{b_2 > \xi, x_2 < l_2^\delta(a_2, b_2, \xi)\}, \\ \mathcal{S}_{2,0}^{a+} &:= \mathcal{C}_{2,0} \cap \{b_2 > \xi, x_2 > l_2^\delta(a_2, b_2, \xi)\}.\end{aligned}\tag{34}$$

Direct fast-slow systems calculations and Fenichel's Theorem yield the next result; see also Figure 5.

Proposition 3.13. *The manifold $\mathcal{C}_{2,0}$ contains a curve of fold points given by*

$$\mathcal{L}_{2,0}^\delta = \{(a_2, b_2, x_2, y_2) \in \mathcal{C}_{2,0} : x_2 = l_2^\delta(a_2, b_2, \xi)\}.$$

For $a_2 \neq 1/(2\xi)$ we have that

- $\mathcal{S}_{2,0}^{\pm}$ are normally hyperbolic of saddle-type,
- $\mathcal{S}_{2,0}^{a\pm}$ are normally hyperbolic attracting.

Furthermore, the manifolds $\mathcal{S}_{2,0}^{r-}$ and $\mathcal{S}_{2,0}^{a+}$ are unbounded as follows

- for $(a_2, b_2, x_2, y_2) \in \mathcal{S}_{2,0}^{r-}$ we have that $(x_2, y_2) \rightarrow (+\infty, +\infty)$ when $(2a_2b_2 - 1) \rightarrow 0$,
- for $(a_2, b_2, x_2, y_2) \in \mathcal{S}_{2,0}^{a+}$ we have that $(x_2, y_2) \rightarrow (+\infty, +\infty)$ when $(2a_2b_2 - 1) \rightarrow 0$.

For $0 < \epsilon \ll 1$ there exist slow manifolds $\mathcal{S}_{2,\epsilon}^{a\pm}$ and $\mathcal{S}_{2,\epsilon}^{r\pm}$. For $\delta = 0$, the curve $\mathcal{L}_{2,0}^\delta$ becomes a line of transcritical points located at $\{b_2 = \xi, x_2 = 0 = y_2\}$.

Remark: We observe that the unbounded structure of the critical manifold for $\delta > 0$, $b_2 < \xi$ resembles closely the autocatalator model [28, 26, 51]. Although we shall not need this observation for the types of periodic orbits considered here, it is likely to be very important for fast dynamics close to the three-dimensional submanifold $\{2a_2b_2 = 1\}$.

Proposition 3.13 already shows that we have to expect several cases for the dynamics in a neighbourhood of $\{b_2 = \xi\}$. For moderate δ bounded away from zero and independent of ϵ , we expect the dynamics to be governed by a jump near a fold. Although it is relevant to observe this mechanism, we shall not discuss this case here as it does not occur for the parameter sets considered by Olsen. For sufficiently small δ , the transcritical singularity is expected to be relevant and the two limiting cases are a jump very close to a transcritical point and canard case with maximal delay.

We start with the singular limit case $\delta = 0$. Then, we find that

$$\mathcal{S}_{2,0}^{a-} = \{(a_2, b_2, x_2, y_2) \in \bar{\mathcal{D}} : x_2 = 0 = y_2, b_2 < \xi\}.$$

In this case, the slow subsystem on $\mathcal{S}_{2,0}^{a-}$ is given by

$$\begin{aligned}\frac{da_2}{ds} &= \mu - \alpha a_2, \\ \frac{db_2}{ds} &= \epsilon b.\end{aligned}\tag{35}$$

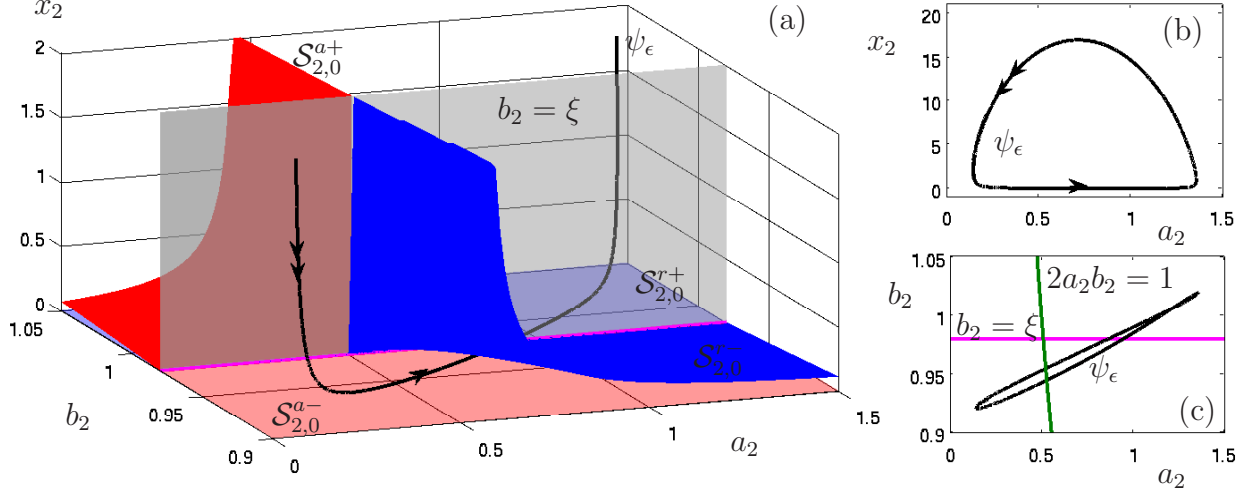


Figure 5: Illustration for the dynamics and fast-slow decomposition of (33). (a) Three-dimensional projection into (a_2, b_2, x_2) -space. For $\delta = 0$, the critical manifolds from Proposition 3.13 (blue=repelling, red=attracting), the transcritical singularities $\mathcal{L}_{2,0}^\delta$ (magenta) and the hyperplane $\{b_2 = \xi\}$ are shown. We also superimpose a truncated periodic solution ψ_ϵ for $k_1 = 0.41$ and standard parameter values as shown in Figure 1(c). (b) Projection of the full periodic solution into (a_2, x_2) -space. (c) Important curves in the (a_2, b_2) -plane.

The a_2 -nullcline is $\{a_2 = \mu/\alpha\}$. Since we consider $\epsilon_b > 0$ as a fixed parameter we can limit our discussion to the case $a^* < a_2(0) < \mu/\alpha$ here. For certain types of MMOs we would need $\epsilon_b \rightarrow 0$; this case is discussed in Section 8. For a given initial condition $(a_2(s_0), b_2(s_0))$ the slow subsystem (35) can be solved explicitly

$$a_2(s) = \frac{\mu}{\alpha} + e^{-\alpha(s-s_0)} \left(a_2(s_0) - \frac{\mu}{\alpha} \right), \quad b_2(s) = \epsilon_b(s - s_0) + b_2(s_0). \quad (36)$$

It is also interesting to see how $\mathcal{C}_{2,0}$ asymptotically depends upon δ in the limit $\delta \rightarrow 0$.

Lemma 3.14. *For $b_2 < \xi$ and $\delta \rightarrow 0$ the attracting manifold $\mathcal{S}_{2,0}^{a-}$ is given by*

$$\begin{aligned} x_2 &= \frac{1}{\xi - b_2} \delta + \frac{1 - 2a_2b_2}{(1 + a_2b_2)(b_2 - \xi)^3} \delta^2 + \mathcal{O}(\delta^3), \\ y_2 &= \frac{1}{(1 + a_2b_2)(b_2 - \xi)^3} \delta^2 + \mathcal{O}(\delta^3), \end{aligned} \quad (37)$$

and the repelling manifold $\mathcal{S}_{2,0}^{a+}$ is given by

$$\begin{aligned} x_2 &= \frac{(1 + a_2b_2)(\xi - b_2)}{2a_2b_2 - 1} + \frac{1}{b_2 - \xi} \delta + \frac{2a_2b_2 - 1}{(1 + a_2b_2)(b_2 - \xi)^3} \delta^2 + \mathcal{O}(\delta^3), \\ y_2 &= \frac{(1 + a_2b_2)(b_2 - \xi)^2}{(1 - 2a_2b_2)^2} + \frac{2}{1 - 2a_2b_2} \delta - \frac{1}{(1 + a_2b_2)(b_2 - \xi)^2} \delta^2 + \mathcal{O}(\delta^3). \end{aligned} \quad (38)$$

Normal hyperbolicity of the critical manifold breaks down along the entire critical manifold $\mathcal{C}_{2,0}$ once it reaches the hyperplane $b_2 = \xi$. Note that the singularity at $(a_2, b_2) = (1/(2\xi), \xi)$ is again particularly degenerate and we exclude the set

$$\mathcal{B}(v) := \left\{ (a_2, b_2, x_2, y_2) \in \bar{\mathcal{D}} : \left(a_2 - \frac{1}{2\xi} \right)^2 + (b_2 - \xi)^2 \leq v \right\} \quad (39)$$

for some small $\nu > 0$ from our analysis as both types of periodic orbits we construct do not have a passage at $(a_2, b_2) = (1/(2\xi), \xi)$ in the singular limit $\epsilon = 0$. As before, we have to make a case distinction. We assume that orbits only approach a neighborhood of $\{b_2 = \xi\}$ via the attracting slow manifolds $\mathcal{S}_{2,0}^{a-}$; see also Figure 5. In the next Section 4 we will consider this case (C1) so that $2a_1^*b_1^* < 1$, $b_1^* < \xi$. For a different case, leading to MMOs, we refer to Section 8.

4 Transcritical Singularities

The slow flow (35) implies that trajectories reach the curve of fold points

$$\mathcal{L}_{2,0}^\delta = \{(a_2, b_2, x_2, y_2) \in \mathcal{C}_{2,0} : x_2 = l_2^\delta(a_2, b_2, \xi)\},$$

which degenerates into a line of transcritical points

$$\mathcal{L}_{2,0}^0 = \{(a_2, b_2, x_2, y_2) \in \mathcal{C}_{2,0} : x_2 = 0 = y_2, b_2 = \xi\}$$

for $\delta = 0$. As in Section 3.2, we shall view δ as a parameter for now. The goal is to compute the unfolding of the degenerate line $\{b_2 = \xi\}$ away from the region $\mathcal{B}(\nu)$. In fact, Lemma 3.14 already indicates that near $b_2 = \xi$, $x_2 = 0 = y_2$ and $\delta = 0 = \epsilon$ a much finer analysis is necessary. In particular, consider the system

$$\begin{aligned} \dot{x}_2 &= 3a_2b_2y_2 - x_2^2 + (b_2 - \xi)x_2 + \delta, \\ \dot{a}_2 &= \epsilon^2(\mu - \alpha a_2 - a_2b_2y_2), \\ \dot{b}_2 &= \epsilon^2\epsilon_b(1 - bx_2 - a_2b_2y_2), \\ \dot{\epsilon} &= 0, \\ \dot{\delta} &= 0, \\ \dot{y}_2 &= \kappa(x_2^2 - y_2 - a_2b_2y_2). \end{aligned} \tag{40}$$

The 6-dimensional flow has to be simplified via center manifold reduction near a line of degenerate equilibrium points

$$\mathcal{L} := \{(x_2, a_2, b_2, \epsilon, \delta, y_2) \in \mathbb{R}^6 : x_2 = 0, a_2 = a_0, b_2 = \xi, \epsilon = 0, \delta = 0, y_2 = 0\}$$

parametrized by a_0 . The necessary calculations are recorded in Appendix D.

Proposition 4.1. *For $a_0 \neq \frac{1}{2\xi}$, there exists a five-dimensional center manifold \mathcal{M}_2 for (40) near \mathcal{L} . The flow on \mathcal{M}_2 is given by*

$$\begin{aligned} \epsilon^2 \frac{dx_2}{ds} &= c_2x_2^2 + c_1(b_2)x_2 + c_0 + \mathcal{O}(3), \\ \frac{da_2}{ds} &= \mu - \alpha a_0 + \mathcal{O}(2), \\ \frac{db_2}{ds} &= \epsilon_b + \mathcal{O}(2), \end{aligned} \tag{41}$$

with $\frac{d\epsilon}{ds} = 0 = \frac{d\delta}{ds}$ understood and $\mathcal{O}(2)$, $\mathcal{O}(3)$ denote higher-order terms of order two and three respectively. Furthermore, the coefficients c_i for $i = \{0, 1, 2\}$ are

$$\begin{aligned} c_2 &= \left(\frac{2a_0\xi - 1}{1 + a_0\xi} \right) > 0, \\ c_1(b_2) &= \left(\frac{-\delta}{\kappa(1 + a_0\xi)^2} + b_2 - \xi \right), \\ c_0 &= \delta + \frac{\delta^2}{\kappa^2(1 + a_0\xi)^3}. \end{aligned}$$

For $\delta = 0$ the system (41) has a line of transcritical singularities at $b_2 = \xi$, as expected. The degenerate singularity at $a_0 = 1/(2\xi)$ also appears and causes a sign change of the x_2^2 -term, which explains why we restrict to dynamics outside of $\mathcal{B}(v)$. We still have the invariant manifolds $\mathcal{S}_{2,\epsilon}^{a\pm}$ and $\mathcal{S}_{2,\epsilon}^{r\pm}$ (up to higher-order correction terms). Then we define

$$\hat{\epsilon} := \epsilon^2 \quad \text{and} \quad \hat{\delta} := \delta/\epsilon^2 = \delta(\sqrt{\hat{\epsilon}})/\hat{\epsilon}. \quad (42)$$

Note that we may always assume that $\hat{\delta}$ is bounded, i.e. $\hat{\delta} = \mathcal{O}(1)$ as $\epsilon \rightarrow 0$, due to the assumptions in Theorem 2.2 in both of the two main cases as either $\delta = \mathcal{O}(e^{-K_1/\epsilon})$ or $\delta = K_2\epsilon^2$. Using (42) in (41) yields

$$\begin{aligned} \hat{\epsilon} \frac{dx_2}{ds} &= f_2(x_2, a_0, b_2; \hat{\epsilon}), \\ \frac{da_2}{ds} &= \mu - \alpha a_0 + \mathcal{O}(2), \\ \frac{db_2}{ds} &= \epsilon_b + \mathcal{O}(2). \end{aligned} \quad (43)$$

where the fast variable vector field is given by

$$\begin{aligned} f_2(x_2, a_0, b_2; \hat{\epsilon}) &= \left(\frac{2a_0\xi - 1}{1 + a_0\xi} \right) x_2^2 + \left(\frac{-\hat{\epsilon}\hat{\delta}}{\kappa(1 + a_0\xi)^2} + b_2 - \xi \right) x_2 \\ &\quad + \hat{\epsilon}\hat{\delta} + \frac{\hat{\delta}^2\hat{\epsilon}^2}{\kappa^2(1 + a_0\xi)^3} + \mathcal{O}(3). \end{aligned} \quad (44)$$

The two normally hyperbolic critical manifolds of (43)

$$\begin{aligned} \mathcal{S}_{2,0}^{r+} &:= \{f_2(x_2, a_0, b_2; 0) = 0, x_2 = 0, b_2 > \xi\}, \\ \mathcal{S}_{2,0}^{a-} &:= \{f_2(x_2, a_0, b_2; 0) = 0, x_2 = 0, b_2 < \xi\}, \end{aligned} \quad (45)$$

are relevant in what follows; note that the definitions agree with the critical manifolds defined in (34) near the transcritical singularity. Next, fix some a_0 such that

$$a_0 > 1/(2\xi). \quad (46)$$

Consider the system (43). The differential equation for a_2 does not enter into the local analysis of the unfolding; this can be seen by applying a change of coordinates

$$a_2 = (\mu - \alpha a_0)(\tilde{a}_2 + \tilde{b}_2), \quad b_2 = \epsilon_b \tilde{b}_2,$$

which implies $\tilde{a}_2' = 0 + \mathcal{O}(2)$ and we can focus on

$$\begin{aligned} \hat{\epsilon} \frac{d\tilde{a}_2}{ds} &= f_2(x_2, a_0, \epsilon_b \tilde{b}_2; \hat{\epsilon}) =: f(x_2, a_0, \tilde{b}_2; \hat{\epsilon}), \\ \frac{d\tilde{b}_2}{ds} &= 1 + \mathcal{O}(2). \end{aligned} \quad (47)$$

In principle, we would have to apply another blow-up to (47) to unfold the transcritical singularity at $\{x_2 = 0, \tilde{b}_2 = \xi/\epsilon_b\}$. However, we are in the fortunate situation that several relevant results are already known for the planar transcritical singularity. Here we follow the results from [46]. The first step is to check whether suitable genericity and transversality conditions [see (2.2)-(2.3) in [46]] hold. The usual transversality condition for the slow

variable holds trivially since $\frac{d\tilde{b}_2}{ds} = 1$. To state the genericity conditions, we use a notational simplification and let $p_{tc} := (0, a_0, \xi/\epsilon_b; 0)$, then the conditions [(2.2), [46]] are given by

$$f(p_{tc}) = 0, \quad \frac{\partial f}{\partial x_2}(p_{tc}) = 0, \quad \frac{\partial f}{\partial \tilde{b}_2}(p_{tc}) = 0, \quad \det((D^2 f)(p_{tc})) < 0, \quad \frac{\partial^2 f}{\partial x_2^2}(p_{tc}) \neq 0. \quad (48)$$

where $D^2 f \in \mathbb{R}^{2 \times 2}$ denotes Hessian matrix with respect to the variables (x_2, \tilde{b}_2) . It is easy to check that the conditions (48) hold. Near a transcritical point, three main dynamical regimes may occur. To distinguish these cases, one possibility is to calculate a particular constant λ_{tc} . To define it, it is helpful to consider the following auxiliary constants

$$c_{xx} := \frac{1}{2} \frac{\partial^2 f}{\partial x_2^2}(p_{tc}), \quad c_{xb} := \frac{1}{2} \frac{\partial^2 f}{\partial x_2 \partial \tilde{b}_2}(p_{tc}), \quad c_{bb} := \frac{1}{2} \frac{\partial^2 f}{\partial \tilde{b}_2^2}(p_{tc}), \quad c_\epsilon := \frac{\partial f}{\partial \hat{\epsilon}}(p_{tc}).$$

Then the key constant λ_{tc} [Lemma 2.1, [46]], in the context of (47), is given by

$$\begin{aligned} \lambda_{tc} &= \frac{1}{\sqrt{c_{xb}^2 - c_{bb}c_{xx}}} (c_\epsilon c_{xx} + c_{xb}) \\ &= \frac{1}{\sqrt{\epsilon_b^2 - 0 \cdot c_{xx}}} \left(\frac{\hat{\delta}}{2} \cdot \frac{2a_0\xi - 1}{1 + a_0\xi} + \epsilon_b \right). \end{aligned}$$

The next result explains the case distinction from Theorem 2.2.

Proposition 4.2. *Consider (43) and suppose (46) holds. Let $\gamma_{\hat{\epsilon}} = \gamma_{\hat{\epsilon}}(s)$ denote a trajectory of (43) starting at some s_0 exponentially close to $\mathcal{S}_{2,\epsilon}^{a,-}$. Then there exists $\hat{\epsilon}_0 > 0$ such that for all $\hat{\epsilon} \in (0, \hat{\epsilon}_0]$ the following cases may occur*

1. **Canard case:** Suppose $\hat{\delta} = \mathcal{O}(e^{-K_1/\hat{\epsilon}})$ and $K_1 > 0$ is some fixed constant independent of $\hat{\epsilon}$. Then $\gamma_{\hat{\epsilon}}$ has a canard segment i.e. it is $\mathcal{O}(\hat{\epsilon})$ -close to $\mathcal{S}_{2,0}^{r,+}$ for a time $s^* = \mathcal{O}(1)$, $s^* > 0$ as $\epsilon \rightarrow 0$.
2. **(Transcritical) jump case:** Suppose $\hat{\delta} = K_2$, $K_2 > 0$ and K_2 is fixed as $\hat{\epsilon} \rightarrow 0$. Then $\gamma_{\hat{\epsilon}}$ does not have a canard segment and leaves $\{x_2 = 0, y_2 = 0\}$ in an $\hat{\epsilon}$ -dependent neighbourhood $\tilde{\mathcal{N}}(\hat{\epsilon})$ of $\{\tilde{b}_2 = \xi/\epsilon_b\}$ such that $d_H(\tilde{\mathcal{N}}(\epsilon), \{b_2 = \xi/\epsilon_b\}) \rightarrow 0$ as $\epsilon \rightarrow 0$.

Proof. Basically, the result follows from [Theorem 2.1, [46]] and the observation that for $\hat{\delta} = \mathcal{O}(e^{-K_1/\hat{\epsilon}})$ the two manifolds $\mathcal{S}_{2,\epsilon}^{a,-}$ and $\mathcal{S}_{2,\epsilon}^{r,+}$ are exponentially close. More precisely, we start with the jump case and observe that

$$\lambda_{tc} = 1 + \frac{K_2}{2\epsilon_b} \cdot \frac{2a_0\xi - 1}{1 + a_0\xi} > 1$$

since $2a_0\xi - 1 > 0$, $K_2 > 0$, $1 + a_0\xi > 0$ and $\epsilon_b > 0$. This implies that we are in the situation of [Theorem 2.1(a), [46]], which implies that a jump occurs near the transcritical point as described in the result we want to prove. The exchange-of-stability case [Theorem 2.1(b), [46]] does not occur as we always have $\lambda_{tc} \geq 1$. For the canard case, observe that for $\hat{\delta} = 0$ the submanifold $\{x_2 = 0 = y_2\}$ is invariant for (40), and hence $\{x_2 = 0\}$ is invariant for (43). Therefore, when $\hat{\delta} = \mathcal{O}(e^{-K_1/\hat{\epsilon}})$ holds, it follows that $\mathcal{S}_{2,\epsilon}^{a,-}$ and $\mathcal{S}_{2,\epsilon}^{r,+}$ are exponentially close. This yields the result for the canard case. \square

For the jump case, there is no further analysis required. Proposition 4.2 implies for this case that we can use the coordinates

$$(a_2(s_1), b_2(s_1), y_2(s_1)) = \left(\frac{\mu}{\alpha} + e^{-\frac{\alpha}{\epsilon b}(\xi - b_2(s_0))} \left(a_2(s_0) - \frac{\mu}{\alpha} \right), \xi, 0 \right) \quad (49)$$

as initial conditions, up to an ϵ -dependent error term, for the slow flow on the critical manifold \mathcal{C}_0 on which large loops occur. This regime is considered in Section 5.

For the canard case, Proposition 4.2 implies that trajectories exponentially close to $\mathcal{S}_{2,\epsilon}^{a-}$ will locally experience maximal delay [58]. However, to verify that there is also global maximal delay, we have to investigate the fast subsystem of (40) linearized around $\{x_2 = 0 = y_2\}$. This linearized system is given by

$$\frac{d}{ds} \begin{pmatrix} X_2 \\ Y_2 \end{pmatrix} = \underbrace{\begin{pmatrix} (b_2 - \xi) & 3a_2b_2, \\ 0 & -(1 + a_2b_2), \end{pmatrix}}_{=: A_{fs}} \begin{pmatrix} X_2 \\ Y_2 \end{pmatrix}. \quad (50)$$

The next result follows from a direct calculation.

Lemma 4.3. *The matrix A_{fs} has eigenvalues $\lambda_{fs,1} = b_2 - \xi$, $\lambda_{fs,2} = -(1 + a_2b_2)$ with associated eigenvectors*

$$\Lambda_{fs,1} = \begin{pmatrix} 1 \\ 0 \end{pmatrix} \quad \text{and} \quad \Lambda_{fs,2} = \begin{pmatrix} -\frac{3a_2b_2}{1+b_2+a_2b_2-\xi} \\ 1 \end{pmatrix}.$$

Furthermore, $\lambda_{fs,1}$ is the critical eigenvalue under suitable conditions i.e.

(E1) $0 \geq \lambda_{fs,1} > \lambda_{fs,2}$ as long as $1 + a_2b_2 + b_2 > \xi$, $b_2 \leq \xi$,

(E2) $0 < \lambda_{fs,1} < |\lambda_{fs,2}|$ as long as $b_2 > \xi$, $-1 - a_2b_2 + b_2 < \xi$.

For standard Olsen parameter values we have $\xi = 0.98$. All candidate orbits we are going to construct below are going to satisfy the conditions on a_2, b_2 (respectively a, b) globally. Therefore, the eigendirection associated to $\lambda_{fs,1}$ is critical, in the sense that the eigenvalue $\lambda_{fs,1}$ is also the weak eigenvalue compared to $\lambda_{fs,2}$.

We may now return to the calculation of the delay time for the canard case. The delay time depends upon the initial conditions using the way-in way-out function [59]

$$\Pi(\gamma_0(s)) := \int_{s_0}^s (D_{x_2} f_2)(\gamma_0(\eta); 0) d\eta.$$

where f_2 is the fast vector field variable from (43). Note that $\Pi(\gamma_0(s_0)) = 0$.

Proposition 4.4. *Suppose (46) holds. Assume $\hat{\delta}(\hat{\epsilon}) = \mathcal{O}(e^{-K_1/\hat{\epsilon}})$ and $\gamma_{\hat{\epsilon}}(s_0)$ is in an $\mathcal{O}(1)$ -neighborhood and the fast-flow basin of attraction for $\mathcal{S}_{2,\epsilon}^{a-}$. Suppose $\gamma_0(s^*) \in \mathcal{L}$ for some $s^* > s_0$ then for times s with*

$$s_0 + \mathcal{O}(\hat{\epsilon} \ln \hat{\epsilon}) \leq s \leq \Pi(s_1) + \mathcal{O}(\hat{\epsilon} \ln \hat{\epsilon})$$

the trajectory $\gamma_{\hat{\epsilon}}(s)$ is in an $\mathcal{O}(\hat{\epsilon})$ -neighborhood of $\mathcal{S}_{2,0}^{r+}$ where $\Pi(s_1) = 0$ and $s_0 < s^ < s_1$.*

Proof. Since solutions do not leave the positive quadrant and we start in $\bar{\mathcal{D}}$, a trajectory can never enter the stable invariant submanifold which is tangent to the local stable eigenspace associated to $\lambda_{fs,2}$ since $\Lambda_{fs,2}$ has always one negative component. Furthermore, the eigenvalue $\lambda_{fs,1}$ is always critical so that we may apply a previous result [Theorem 2.4, [65]; see also [55] where the result was proven first]. The logarithmic corrections of the transition time, calculated using the way-in way-out function, is a direct consequence of the calculation in [59]. \square

In analogy to the jump case (49), we also want to compute the departure point $\gamma_0(s_1)$ in $\mathcal{S}_{2,0}^+$ for the canard case in the singular limit. In view of Proposition 4.4, we have to evaluate the way-in way-out function.

Corollary 4.5. *Under the same assumptions as in Proposition 4.4 the point $\gamma_0(s_1)$ is given by*

$$\gamma_0(s_1) = \left(\frac{\mu}{\alpha} + e^{-\alpha(2/\epsilon_b(\xi - b_2(s_0)))} \left(a_2(s_0) - \frac{\mu}{\alpha} \right), 2\xi - b_2(s_0), 0, 0 \right). \quad (51)$$

Proof. A direct calculation yields

$$\begin{aligned} \int_{s_0}^s D_{x_2} f_2(\gamma_0(\eta); 0) d\eta &= \int_{s_0}^s (b_2(\eta) - \xi) d\eta \\ &= \int_{s_0}^s (\epsilon_b \eta + b_2(s_0) - \xi) d\eta \\ &= \epsilon_b \frac{1}{2} (s - s_0)^2 + (b_2(s_0) - \xi)(s - s_0). \end{aligned}$$

For $s_1 > s_0$ we find that $\Pi(\gamma_0(s_1)) = 0$ if $s_1 = 2/\epsilon_b(\xi - b_2(s_0)) + s_0$. Using the solution (36) of the slow subsystem (35) and substituting the result for s_1 yields (51). \square

Proposition 4.2 and Corollary 4.5 imply that we can use the coordinates

$$(a_2(s_1), b_2(s_1), y_2(s_1)) = \left(\frac{\mu}{\alpha} + e^{-\alpha(2/\epsilon_b(\xi - b_2(s_0)))} \left(a_2(s_0) - \frac{\mu}{\alpha} \right), 2\xi - b_2(s_0), 0 \right) \quad (52)$$

as initial condition, up to an ϵ -dependent error term, in the canard case for the slow flow on the critical manifold \mathcal{C}_0 on which large loops occur. This regime is considered in Section 5.

5 Large Loops

We return to the analysis of the slow flow on the critical manifold \mathcal{C}_0 from Section (2). The flow is given by

$$\begin{aligned} \frac{da}{d\tau} &= -aby, \\ \frac{db}{d\tau} &= -\epsilon_b aby, \\ \frac{dy}{d\tau} &= \kappa(2ab - 1)y. \end{aligned} \quad (53)$$

Proposition 5.1. *The slow flow (53) is solved by*

$$b = \epsilon_b a + K_1 \quad \text{and} \quad y = K_2 + \kappa \left(-2a + \frac{\ln a}{K_1} - \frac{\ln(K_1 + a\epsilon_b)}{K_1} \right) \quad (54)$$

for constants $K_{1,2}$ to be determined from the initial conditions.

Proof. From the first two equations in (53) it follows that

$$\frac{db}{da} = \epsilon_b \quad \Rightarrow \quad b = \epsilon_b a + K_1$$

for some constant K_1 . Inserting this result in the first and third equation of (53) yields

$$\frac{dy}{da} = -\kappa \frac{2a(\epsilon_b a + K_1) - 1}{a(\epsilon_b a + K_1)} = -2\kappa + \frac{\kappa}{a(\epsilon_b a + K_1)}. \quad (55)$$

The result follows upon solving (55) explicitly. \square

Proposition 5.1 resolves the global large return dynamics for x, y . However, we still need to consider the solution (54) in even more detail. It is going to be helpful to extract as much relevant information from the explicit solution (54) analytically as possible to prove results about oscillations in the Olsen model. The main case we are interested in is an initial condition

$$(a(0), b(0), y(0)) = (\alpha_1, \beta_1, 0) \quad (56)$$

corresponding to a singular loop starting at a fold point. The choice of subscripts in (56) will become clear in Section 6. We are most interested in the two cases when (56) is either given by (49) for the jump case, or by (52) in the canard case.

From (56) and (54) it follows that $\beta_1 - \epsilon_b \alpha_1 = K_1$. Furthermore, for (55) the initial condition is $y(\alpha_1) = 0$. Direct calculations yield

$$y(a) = \frac{\kappa}{\beta_1 - \epsilon_b \alpha_1} \left[2(a - \alpha_1)(\alpha_1 \epsilon_b - \beta_1) + \ln \left(\frac{\beta_1 a}{\alpha_1(\beta_1 + \epsilon_b(a - \alpha_1))} \right) \right], \quad (57)$$

where we have to assume $\alpha_1(\beta_1 + \epsilon_b(a - \alpha_1)) \neq 0$; this last assumption will always be satisfied for standard Olsen parameter values in the region of interest for candidate orbits we want to construct. Indeed, note that we always have positive $a, \alpha_1 = \mathcal{O}(1)$ and $b > b^*$ is bounded away from zero by a suitable constant $b^* > 0$.

Now observe carefully that the singular (or candidate) loops are restricted to a family of invariant lines upon projection into the (a, b) -plane

$$\{(a, b, x, y) \in \mathcal{D} : x = 0 = y, b = \epsilon_b a + \beta_1 - \epsilon_b \alpha_1\}. \quad (58)$$

We collect some important information on the function $y(a)$.

Lemma 5.2. *Considering (57) we have*

$$y'(a) = \frac{(1 - 2a(\beta_1 + (a - \alpha_1)\epsilon_b)\kappa}{a(\beta_1 + (a - \alpha_1)\epsilon_b)}, \quad \text{so that } y'(\alpha_1) = \frac{\kappa(1 - 2\alpha_1\beta_1)}{\alpha_1\beta_1}.$$

Assume $\beta_1 - \alpha_1\epsilon_b > 0$ and standard parameter values then $y(a)$ has local extrema at

$$a_{\pm} = \frac{2\alpha_1\epsilon_b - 2\beta_1 \pm \sqrt{8\epsilon_b + (2\alpha_1\epsilon_b - 2\beta_1)^2}}{4\epsilon_b}$$

with $a_+ > 0$, $a_- < 0$, $y(a_+) \geq 0$. For $a \in [0, +\infty)$ one finds that a_+ is a global maximum, $a_+ < \alpha_1$ for $2\alpha_1\beta_1 - 1 > 0$, $y(a_+) = 0$ if and only if $2\alpha_1\beta_1 - 1 = 0$ and $y(a_+) > 0$ for $2\alpha_1\beta_1 - 1 \neq 0$. Furthermore, we have the asymptotics

$$\lim_{a \rightarrow 0^+} y(a) = -\infty \quad \text{and} \quad \lim_{a \rightarrow +\infty} y(a) = -\infty.$$

We restrict to loops for $y(\alpha_1) = 0$ when $2\alpha_1\beta_1 - 1 > 0$ based upon the results in Section 4. From Lemma 5.2 it follows that there exists another zero α_2 such that $y(\alpha_2) = 0$ and $\alpha_2 < a_+ < \alpha_1$. Therefore, Lemma 5.2 provides a rigorous justification for the trajectories shown in Figure 3(a) which make large excursions, with a single maximum, in \mathcal{C}_0 . To compute the landing point α_2 we must solve the equation

$$y(\alpha_2) = 0 \quad \Leftrightarrow \quad 2(\alpha_2 - \alpha_1)(\beta_1 - \alpha_1\epsilon_b) = \ln \left(\frac{\beta_1\alpha_2}{\alpha_1(\beta_1 + \epsilon_b(\alpha_2 - \alpha_1))} \right) \quad (59)$$

which is transcendental and the solutions cannot be given in closed form. Despite this problem one can still use (59) to construct candidate orbits.

6 Construction of Candidate Orbits

In this section we construct global candidate orbits for the jump case and the canard case. Since there are two different starting points for the large loops to consider, i.e. either (49) or (52), we subdivide the following discussion into two cases.

6.1 A Canard Candidate

The canard case is more difficult so we shall discuss it first, and in more detail. The candidate orbit we aim to construct consists of a concatenation of a slow flow segment defined by (35) on the time scale s with maximal delay and a fast segment on the time scale $\tau = \epsilon^{-2}s$ for (6). Both segments are constructed in the singular limit for $\epsilon = 0$ with $\epsilon_b > 0$. The fast segment is itself a slow segment for the subsystem (53) on the attracting critical manifold \mathcal{C}_0 ; see also Figure 3(a).

Let (α_0, β_0) denote an initial condition for (35) with $2\alpha_0\beta_0 < 1$ and $\beta_0 < \xi$. By Corollary 4.5 the maximal delay point (α_1, β_1) is given by

$$\alpha_1 = \frac{\mu}{\alpha} + e^{-\alpha(2/\epsilon_b(\xi - \beta_0))} \left(\alpha_0 - \frac{\mu}{\alpha} \right), \quad (60)$$

$$\beta_1 = 2\xi - \beta_0. \quad (61)$$

Augmenting this point by the trivial condition $y = 0$ gives $(\alpha_1, \beta_1, 0) = (a, b, y)$ which is the initial condition for the slow flow (53) governing the large loop. By Proposition 5.1 and equation (59) the conditions

$$0 = 2(\alpha_2 - \alpha_1)(\beta_1 - \alpha_1\epsilon_b) - \ln \left(\frac{\beta_1\alpha_2}{\alpha_1(\beta_1 + \epsilon_b(\alpha_2 - \alpha_1))} \right), \quad (62)$$

$$\beta_1 = \epsilon_b\alpha_1 + \beta_2 - \epsilon_b\alpha_2 \quad (63)$$

follow, where (63) is the requirement to lie in a single invariant line (58). For a periodic candidate orbit we must have

$$(\alpha_0, \beta_0) \stackrel{!}{=} (\alpha_2, \beta_2). \quad (64)$$

Substituting (64) into (60)-(63) yields a nonlinear system of four algebraic equations in four unknowns $(\alpha_0, \beta_0, \alpha_1, \beta_1)$.

Lemma 6.1. *The system (60)-(64) can be simplified to a single algebraic equation for β_0 given by*

$$0 = 4(\beta_0 - \xi)(\epsilon_b \mu - \alpha \xi) + 4(\beta_0 - \xi)w_c(\beta_0) + \alpha \epsilon_b \ln \left[\frac{(2\xi - \beta_0)(\beta_0 \alpha + \epsilon_b \mu - \alpha \xi + w_c(\beta_0))}{\beta_0 (\epsilon_b \mu - \alpha \beta_0 + \alpha \xi + w_c(\beta_0))} \right] =: W_c(\beta_0) \quad (65)$$

where $w_c(\beta_0) := \alpha(\beta_0 - \xi) \coth \left[\frac{\alpha(\xi - \beta_0)}{\epsilon_b} \right]$.

Proof. Replace β_1 in (62) and (63) using (61) which only depends on β_0 . Then replace α_1 in (62) and (60) using (63) i.e. $(2\xi - 2\beta_0 + \epsilon_b \alpha_0)/\epsilon_b = \alpha_1$. Then notice that (60) can be solved for α_0

$$\alpha_0 = \frac{\beta_0 \alpha + \epsilon_b \mu - \alpha \xi + \alpha(\beta_0 - \xi) \coth[\alpha(\xi - \beta_0)/\epsilon_b]}{\alpha \epsilon_b}. \quad (66)$$

Substituting (66) into (62) gives the result. \square

Hence we have to determine whether $W_c(\beta_0)$ has a zero, which also satisfies the relevant constraints as an arrival point for a large loop, i.e. we need

$$\beta_0 < \xi \quad \text{and} \quad 2\alpha_0 \beta_0 = \frac{2\beta_0}{\alpha \epsilon_b} (\beta_0 \alpha + \epsilon_b \mu - \alpha \xi + w_c(\beta_0)) < 1. \quad (67)$$

This requires a better understanding of the function W_c . Having reduced the problem to a single algebraic equation, we could investigate W_c numerically. However, it is even possible to obtain analytical results. We view μ as a parameter that we may adjust to find the required root.

Lemma 6.2. *The following properties hold:*

(P1) $W_c(\xi) = 0$.

(P2) $\frac{dW_c}{d\beta_0}(\xi) = W'_c(\xi) = \frac{2}{\xi}(\epsilon_b - \epsilon_b \mu + \alpha \xi)(\alpha - 2(\mu - 1)\xi)(\mu - 1)^{-1}$.

(P3) *Suppose that $\epsilon_b, \alpha, \xi, \mu > 0$. Then $W'_c(\xi) < 0$ if and only if one of the following three cases holds*

$$\begin{aligned} (i) \quad & 0 < \mu < 1, \quad \alpha > -2\xi + 2\mu\xi, \\ (ii) \quad & 1 < \mu < \frac{\alpha+2\xi}{2\xi}, \quad \epsilon_b > \frac{\alpha\xi}{\mu-1}, \\ (iii) \quad & \mu > \frac{\alpha+2\xi}{2\xi}, \quad 0 < \epsilon_b < \frac{\alpha\xi}{\mu-1}. \end{aligned}$$

Consider μ as a parameter and otherwise standard parameter values from Table 2 ($k_1 = 0.41$). Then the following results hold:

(P4) If $0 < \mu < 1$ then $W_c(\beta_0) \neq 0$ for $\beta_0 \in (0, \xi)$.

(P5) There exists an open set (μ_1, μ_2) with $1 < \mu_1 < \mu_2$ such that if $\mu \in (\mu_1, \mu_2)$ then $W_c(\beta_0^*) = 0$ for some $0 < \beta_0^* < \xi$.

Proof. (P1) and (P2) follow from a direct limit calculation. (P3) is a corollary of (P2). (P4) can be proven via a geometric argument: The invariant lines (58) have slope $m_1 = \epsilon_b$ as functions of a . The slow flow (35) is affine with direction $(\mu - \alpha a, \epsilon_b)^T$ so that locally we have a slope $m_2 = \epsilon_b/(\mu - \alpha a)$. A canard candidate of the prescribed form certainly requires $m_1 > m_2$ at the point (α_0, β_0) as a trajectory of (35) must intersect a single invariant line (58) twice. Hence, $\epsilon_b > \epsilon_b/(\mu - \alpha_0 a)$ and so $\mu - \alpha_0 a > 1$; even if α_0 is very small we need at least $\mu > 1$ which proves (P3).

Regarding (P5), we first observe that (P4) implies we have to restrict to the case $\mu \geq 1$ to find a root. Then we consider (P3) and observe that $W'_c(\xi) < 0$ if and only if (P3)(iii) holds (which actually yields a bound $\mu > 233/196$). If we can show that there exists $\beta_0 \in (0, \xi)$ such that $W_c(\beta_0) < 0$, then the intermediate value theorem will yield the required root, as well as the open set of μ -parameter values. To show this, consider one part of the argument of the logarithmic term in W_c given by

$$w_{\text{aux}}(\beta_0) := \epsilon_b \mu + \alpha(\beta_0 - \xi) + w_c(\beta_0).$$

We may directly check that $w_{\text{aux}}(\xi) = \epsilon_b(\mu - 1) > 0$ and there exists $\beta_0 < \xi$ such that $w_{\text{aux}}(\beta_0) < 0$ e.g. $w_{\text{aux}}(\beta_0 - \epsilon_b/\alpha) = \mu - 1 - \coth(1)$ so that there exists an open set of μ -values for which $\mu > 233/196$ and $\mu - 1 - \coth(1) < 0$. The intermediate value theorem implies that there exists β_{00} such that $w_{\text{aux}}(\beta_{00}) = 0$. Using another direct calculation, we see that the term $w_{\text{aux}}(\beta_0)$ dominates in the exponential and it follows that $\lim_{\beta_0 \rightarrow \beta_{00}} W_c(\beta_0) = -\infty$. Hence, there exists a β_0^* with $\beta_0^* < \xi$ such that $W(\beta_0^*) = 0$. \square

Of course, the result (P5) above is not very explicit and could potentially be improved. However, we do not think it is possible to provide a full classification of all periodic solutions based upon all the system parameters analytically. To explore various quantitative bounds for parameter ranges, it seems more adequate to use numerical methods, such as numerical continuation [15, 14]. Here we only provide a proof of the main geometric structure. Lemma 6.2 implies the existence of a candidate orbit for the canard case of Theorem 2.2.

Corollary 6.3. *There exists an open set $(\mu_{c,1}, \mu_{c,2})$ with $\mu_{c,1} < \mu_{c,2}$ such that the Olsen model (6), for $\mu \in (\mu_{c,1}, \mu_{c,2})$ and otherwise standard parameter values from Table 1 ($k_1 = 0.41$), has a periodic candidate orbit ψ_0 . It consists of two segments, one for the slow flow (35) including a canard segment and one consisting of a large loop defined by (53).*

Corollary 6.3 is a singular limit result for $\epsilon = 0$. Therefore, we still have to show that the candidate orbit indeed perturbs to an actual periodic orbit for $0 < \epsilon \ll 1$. This step, which is actually the reason why we use the blow-up technique, is carried out in Section 7. We refer to the candidate orbit from Corollary 6.3 as a candidate of a non-classical relaxation oscillation. Indeed, comparing with the classical relaxation oscillation case [24], one immediately notices that our construction here still has a ‘fast’ phase corresponding to the large loop and a ‘slow’ phase corresponding to a sliding-type motion near the fold

locus. However, the critical manifold structure(s) as well as the fast-slow decomposition differ substantially from the cubic or S-shaped critical manifold of classical relaxation oscillations; see also Figure 5.

6.2 A Jump Candidate

The next step is to also consider the jump case from Proposition 4.2 in combination with the large loops. The jump candidate orbit consists of a concatenation of a slow flow segment defined by (35) on the time scale s up to $b_2 = \xi$ and a fast segment on the time scale $\tau = \epsilon^{-2}s$ for (6); see also Figure 3(a).

As in Section 6.1, let (α_0, β_0) denote an initial condition for (35) with $2\alpha_0\beta_0 < 1$ and $\beta_0 < \xi$. The departure point (α_1, β_1) for the jump case is calculated in (49). Analogously, to (60)-(63) we get four algebraic equations

$$\alpha_1 = \frac{\mu}{\alpha} + e^{-\frac{\alpha}{\epsilon_b}(\xi - \beta_0)} \left(\alpha_0 - \frac{\mu}{\alpha} \right), \quad (68)$$

$$\beta_1 = \xi, \quad (69)$$

$$0 = 2(\alpha_2 - \alpha_1)(\beta_1 - \alpha_1\epsilon_b) - \ln \left(\frac{\beta_1\alpha_2}{\alpha_1(\beta_1 + \epsilon_b(\alpha_2 - \alpha_1))} \right), \quad (70)$$

$$\beta_1 = \epsilon_b\alpha_1 + \beta_2 - \epsilon_b\alpha_2. \quad (71)$$

For a periodic candidate orbit we must again impose

$$(\alpha_0, \beta_0) \stackrel{!}{=} (\alpha_2, \beta_2). \quad (72)$$

Substituting (72) into (68)-(71) yields a nonlinear system of four algebraic equations in four unknowns $(\alpha_0, \beta_0, \alpha_1, \beta_1)$.

Lemma 6.4. *The system (68)-(72) can be simplified to a single algebraic equation for β_0 given by*

$$\begin{aligned} 0 = & 2(\beta_0 - \xi) (\epsilon_b\mu - \alpha\xi + \alpha(\beta_0 - \xi)/w_j(\beta_0)) \\ & + \alpha\epsilon_b \ln \left(\frac{\xi(\mu\epsilon_bw_j(\beta_0) + \alpha(\beta_0 - \xi) \exp[\alpha(\xi - \beta_0)/\epsilon_b])}{\beta_0(\mu\epsilon_bw_j(\beta_0) + \alpha(\beta_0 - \xi))} \right) =: W_j(\beta_0) \end{aligned} \quad (73)$$

where $w_j(\beta_0) := \exp[\alpha(\xi - \beta_0)/\epsilon_b] - 1$.

Proof. Similar steps as in the proof of Lemma 6.1 are required. We have to replace the algebraic equations (60)-(61) by (68)-(69) and carry out lengthy, albeit quite direct, algebraic manipulations to obtain (73). \square

The next result follows from a direct calculation using (73) which we omit here for brevity.

Lemma 6.5. *The properties (P1)-(P5) from Lemma 6.2 hold verbatim if W_c is replaced by W_j .*

In fact, note that the arguments in Lemma 6.2 only depend upon the sign of the derivative $W'_c(\xi)$ and the asymptotic behaviour of the logarithmic summand in W_c . Lemma 6.5 states that the same technique can also be applied to W_j . From this last observation, the next two result follow immediately.

Corollary 6.6. *There exists an open set $(\mu_{j,1}, \mu_{j,2})$ with $\mu_{j,1} < \mu_{j,2}$ such that the Olsen model (6), for $\mu \in (\mu_{j,1}, \mu_{j,2})$ and otherwise standard parameter values from Table 1 ($k_1 = 0.41$), has a periodic candidate orbit ψ_0 . It consists of two segments, one for the slow flow (35) without a canard segment and one consisting of a large loop defined by (53).*

Corollary 6.7. *The open sets $(\mu_{c,1}, \mu_{c,2})$ from Corollary 6.3 and $(\mu_{j,1}, \mu_{j,2})$ Corollary 6.6 have a non-empty intersection i.e. there exists an open set (μ_1, μ_2) with $\mu_1 < \mu_2$ such that $(\mu_1, \mu_2) \subseteq (\mu_{j,1}, \mu_{j,2}) \cap (\mu_{c,1}, \mu_{c,2})$.*

Essentially, Corollary 6.7 states that δ may deform a canard-type orbit with maximal delay into an orbit which jumps near the transcritical singularity; see also the discussion in Section 2 following equation (11). As before, we are not interested here in any sharp quantitative bounds for μ_1, μ_2 in Corollary 6.7.

7 The Return Map

The last step is to construct the global return map using the result from Sections 3-4 to obtain perturbation of the canard candidate orbits constructed in Sections 5-6. As in Section 6, we are going to split the analysis of the return map into the two main cases from Theorem 2.2.

7.1 The Canard Case

Before we can analyze the full return map several auxiliary results on the slow flow (35) are needed. Let $\phi_c : [a^*, \infty) \times [b^*, \xi) \rightarrow [a^*, \infty) \times [\xi, \infty)$ denote the slow flow map with maximal delay for an initial condition (a, b) with $2ab < 1$ and $b < \xi$ so that

$$\phi_c(a, b) = \left(\frac{\mu}{\alpha} + e^{-\frac{2\alpha}{c_b}(\xi-b)} \left(a - \frac{\mu}{\alpha} \right), 2\xi - b \right).$$

We assume that μ is chosen so that the candidate orbit constructed in Section 6.1 exists. Let (α_0, β_0) denote the landing point of this singular periodic orbit on $\mathcal{S}_{2,0}^{a-}$ and, as before, let $(\alpha_1, \beta_1) = \phi_c(\alpha_0, \beta_0)$; see also Figure 6.

Lemma 7.1. *Let $\rho > 0$ be sufficiently small then for $\phi_c(\alpha_0, \beta_0 - \rho) = (\alpha_{1*}, \beta_{1*})$ we have $\beta_{1*} > \beta_1$ and for $\phi_c(\alpha_0, \beta_0 + \rho) = (\alpha_1^*, \beta_1^*)$ we have $\beta_1^* < \beta_1$.*

Proof. Under maximal delay we get $\beta_{1*} = 2\xi - \beta_0 + \rho > 2\xi - \beta_0 = \beta_1$ and for the second part $\beta_1^* = 2\xi - \beta_0 - \rho < 2\xi - \beta_0 = \beta_1$. \square

We know that the canard candidate periodic orbit exists for $\beta_0 < \xi$ under suitable conditions on μ . The next result analyzes the slow dynamics of points near the candidate orbit in more detail, which will be important for the stability of the periodic orbit.

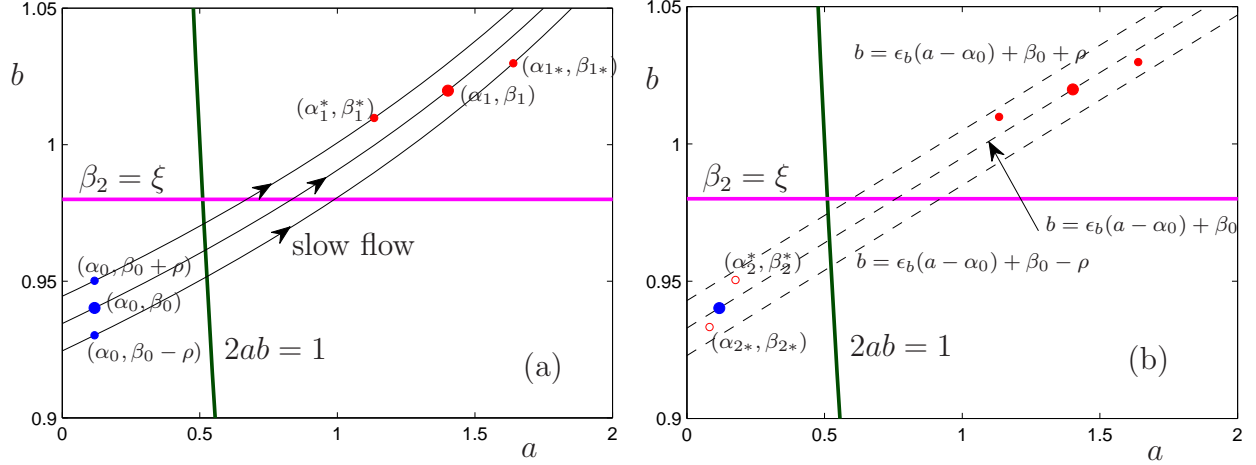


Figure 6: Numerical illustration of the results from Lemma 7.1 and Lemma 7.2; slow flow map for the canard case. Parameter values are $\epsilon_b = 0.062$, $\kappa = 3.93$, $\xi = 0.98$, $\alpha = 0.37$, $\mu = 1.3$. (a) Slow subsystem phase space with three orbits (black curves) containing the three points (blue) $a = \alpha_0$, $b = \beta_0 - \rho, \beta_0, \beta_0 + \rho$ for $\rho = 0.01$ with $\alpha_0 \approx 0.1176$ and $\beta_0 \approx 0.9402$. The image points under the slow flow map ϕ_c with maximal delay (red) are shown as well. (b) Phase space with the three invariant lines (dashed black, defined by (58)). The thick points (blue/red) correspond to the singular periodic orbit whereas the two circles (red) correspond to the images under the global map defined by (53).

Lemma 7.2. *Under the assumptions of Lemma 7.1 we find that*

$$\beta_{1*} > \epsilon_b \alpha_{1*} + \beta_0 - \rho - \epsilon_b \alpha_0 \quad \text{and} \quad \beta_1^* < \epsilon_b \alpha_1^* + \beta_0 + \rho - \epsilon_b \alpha_0.$$

Proof. Recall that the candidate orbit is given by the condition

$$\beta_1 = \epsilon_b \alpha_1 + \beta_0 - \epsilon_b \alpha_0.$$

The slow flow on $\{x_2 = 0 = y_2\}$ is two-dimensional, so trajectories cannot intersect by uniqueness. Consider the slow flow trajectory $\gamma = \gamma(s)$ starting at $(\alpha_0, \beta_0 - \rho) = \gamma(0)$. Observe that $\gamma(s)$ lies below the line given by $\beta = \epsilon_b \alpha_1 + \beta_0 - \rho - \epsilon_b \alpha_0$ for $0 < s \ll 1$ and has to cross this line again so that it is close to the point (α_1, β_1) ; see also Figure 6. Note that we have used that ρ is sufficiently small in the last step. The geometric crossing condition is equivalent to the algebraic condition

$$\beta_{1*} > \epsilon_b \alpha_{1*} + \beta_0 - \rho - \epsilon_b \alpha_0$$

as shown in Figure 6(b). The second part is proven similarly, except that we notice that a trajectory starting at $(\alpha_0, \beta_0 + \rho)$ must lie below the line $\beta = \epsilon_b \alpha_1 + \beta_0 + \rho - \epsilon_b \alpha_0$ when it reaches a neighbourhood of (α_1, β_1) . \square

Finally, we can proceed to prove the first part of the main result.

Proof. (of Theorem 2.2, canard case) The existence of the candidate ψ_0 is just a consequence of Corollary 6.3. To analyze the perturbation $\epsilon \in (0, \epsilon_0]$, we have to consider the global

Poincaré map near the candidate orbit ψ_0 . Fix a suitable small $\rho > 0$ and define a cross-section

$$\Sigma_0 := \{(a, b, x, y) \in \bar{\mathcal{D}} : a = \alpha_0 + \rho, b \in [\beta_0 - \rho, \beta_0 + \rho], x \in [0, \rho], y \in [0, \rho]\},$$

which is transverse to the flow on $\mathcal{S}_{2,\epsilon}^{a-}$; the existence of such a section follows from Proposition 3.13, Fenichel theory and the transversality of the slow flow on $\mathcal{S}_{2,0}^{a-}$ to $\{a = \alpha_0, b \in [\beta_0 - \rho, \beta_0 + \rho]\}$. Define another section

$$\Sigma_1 := \left\{ (a, b, x, y) \in \bar{\mathcal{D}} : a \in [\alpha_1 - \rho, \alpha_1 + \rho], b \in [\beta_1 - \rho, \beta_1 + \rho], x = k\epsilon, y = \frac{x^2}{3ab} \right\},$$

where $k > 0$ is a suitable constant. The flow induced map $\phi_{01} : \Sigma_0 \rightarrow \Sigma_1$ is a diffeomorphism due the canard case from Proposition 4.2 and since the exit from $\mathcal{S}_{2,\epsilon}^{r+}$ is described by the center flow in chart κ_1 in Proposition 3.10(C4). For the global returns consider the section

$$\Sigma_2 := \left\{ (a, b, x, y) \in \bar{\mathcal{D}} : a \in [\alpha_0 - \rho, \alpha_0 + \rho], b \in [\beta_0 - \rho, \beta_0 + \rho], x = k\epsilon, y = \frac{x^2}{3ab} \right\}.$$

The flow induced map $\phi_{01} : \Sigma_1 \rightarrow \Sigma_2$ is a diffeomorphism by Fenichel's Theorem applied to \mathcal{C}_0 . The global flow is approximated by the flow on attracting slow manifold \mathcal{C}_ϵ which makes Proposition 5.1 applicable. Since $2\alpha_0\beta_0 < 1$ and $\beta_0 < \xi$, it follows from Proposition 3.10(C1) that $\phi_{2,0} : \Sigma_2 \rightarrow \Sigma_0$ is a diffeomorphism defined via trajectories following the dynamics of the center-stable manifold \mathcal{M}_1 in the chart κ_1 . Note that Σ_0 is slightly shifted with $a = \alpha_0 + \rho$ from the base point of the candidate orbit to avoid that points of the global large loops land exactly on the section. The global return map

$$\phi = \phi_{20} \circ \phi_{12} \circ \phi_{01} : \Sigma_0 \rightarrow \Sigma_0 \quad (74)$$

is exponentially contracting in the (x, y) -directions since (I) \mathcal{C}_ϵ for (x, y) bounded away from $(0, 0)$ is attracting, (II) trajectories follow $\mathcal{S}_{2,0}^{a-}$ and $\mathcal{S}_{2,0}^{r+}$ in the chart κ_2 and (III) trajectories connect to \mathcal{C}_ϵ in the entrance and exit chart κ_1 . If we can show that the map ϕ also contracts along the b -direction the result will follow.

The contraction in the b -direction can be derived by using Lemmas 7.1-7.2. Indeed, consider first the point $(\alpha_0, \beta_0 - \rho)$ then by Lemma 7.2 the image $(\alpha_{1*}, \beta_{1*}) = \phi_c(\alpha_0, \beta_0 - \rho)$ lies between the lines which are invariants for (α_0, β_0) and $(\alpha_0, \beta_0 - \rho)$ for the global flow from Proposition 5.1; see also Figure 6. By Lemma 5.2 the global return of $(\alpha_{1*}, \beta_{1*})$ governed by the flow on \mathcal{C}_0 ends at a point $(\alpha_{2*}, \beta_{2*})$ with $\alpha_{2*} < \alpha_0$ which again lies between the same two lines. The slow flow from $(\alpha_{2*}, \beta_{2*})$ back to a section $\{a = \alpha_0, b \in [\beta_0 - \rho, \beta_0]\}$ does not change this property since the b -coordinate on $\mathcal{S}_{2,\epsilon}^{a-}$ increases.

For sufficiently small ρ the same argument applies for a point $(\alpha_0 + \rho, \beta_0 - \rho) \in \Sigma_0$. Indeed, as for $(\alpha_0, \beta_0 - \rho)$ one may consider a point $(\alpha_0, \beta_0 + \rho)$ with the minor modification that we start with a point in the interior of the open set between (α_0, β_0) and $(\alpha_0, \beta_0 + \rho)$ in Σ_0 and argue in backward-time i.e. points with fixed α_0 lying above (α_0, β_0) move away from the β_0 in backward time. The same applies for points with $\alpha_0 + \rho$ lying on Σ_0 .

Hence the full map ϕ also contracts along the b -direction. The existence of an attracting fixed point now follows, e.g. from the Banach fixed point theorem. This fixed point is precisely the intersection of an orbit ψ_ϵ with Σ_0 . \square

In the proof we could have inserted another section between Σ_0 and Σ_1 to describe the exit to \mathcal{C}_ϵ via Proposition 3.10(C4) separately. Alternatively, we could also have removed Σ_2 and treated the transition map from Σ_1 to Σ_0 at once.

7.2 The Jump Case

Although a similar argument as for the canard case can be followed, we have to replace Lemma 7.1 and 7.2. Consider the slow flow (35) and let $\phi_j : [a^*, \infty) \times [b^*, \xi) \rightarrow [a^*, \infty) \times [\xi, \infty)$ denote the slow flow map for the jump case for an initial condition (a, b) with $2ab < 1$ and $b < \xi$ so that

$$\phi_j(a, b) = \left(\frac{\mu}{\alpha} + e^{-\frac{\alpha}{\epsilon_b}(\xi-b)} \left(a - \frac{\mu}{\alpha} \right), \xi \right).$$

We assume that μ is chosen so that the candidate orbit constructed in Section 6.2 exists. Let (α_0, β_0) denote the landing point of this singular periodic orbit on $\mathcal{S}_{2,0}^{a-}$ and, as before, let $(\alpha_1, \beta_1) = \phi_j(\alpha_0, \beta_0)$; see also Figure 7. Note that we always have $\beta_1 = \xi$ for the jump case and hence we do not have to control the b -coordinate.

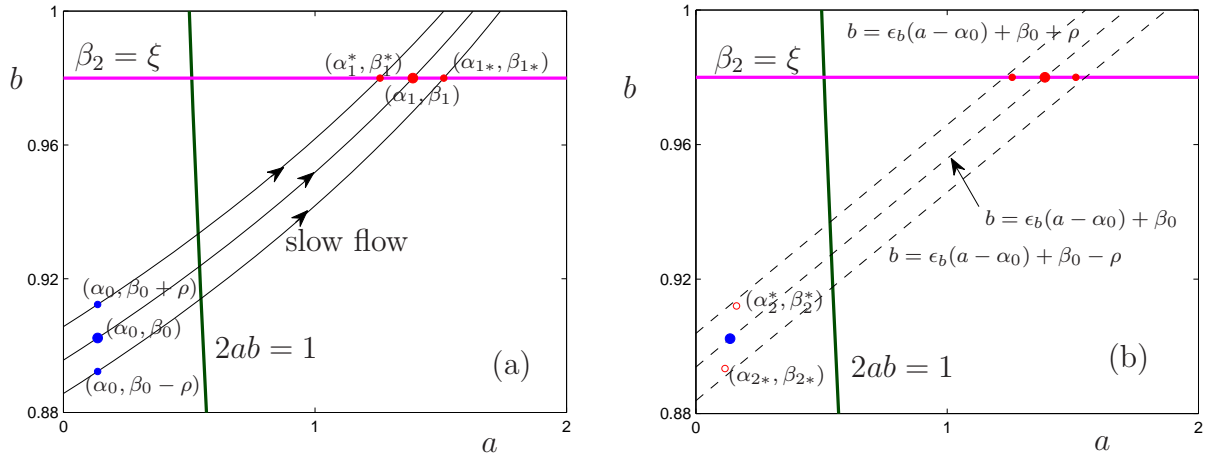


Figure 7: Numerical illustration of the results from Lemma 7.3; slow flow map for the jump case. Parameter values are $\epsilon_b = 0.062$, $\kappa = 3.93$, $\xi = 0.98$, $\alpha = 0.37$, $\mu = 1.3$. (a) Slow subsystem phase space with three orbits (black curves) containing the three points (blue) $a = \alpha_0$, $b = \beta_0 - \rho, \beta_0, \beta_0 + \rho$ for $\rho = 0.01$ with $\alpha_0 \approx 0.1362$ and $\beta_0 \approx 0.9023$. The image points under the slow flow map ϕ_j (red) are shown as well. (b) Phase space with the three invariant lines (dashed black, defined by (58)). The thick points (blue/red) correspond to the singular periodic orbit whereas the two circles (red) correspond to the images under the global map defined by (53).

Lemma 7.3. *Let $\rho > 0$ be sufficiently small and let $\phi_j(\alpha_0, \beta_0 - \rho) = (\alpha_{1*}, \xi)$ and $\phi_c(\alpha_0, \beta_0 + \rho) = (\alpha_1^*, \xi)$. Then we have*

$$\frac{1}{\epsilon_b}(\xi - \beta_0 + \rho + \epsilon_b \alpha_0) > \alpha_{1*} \quad \text{and} \quad \frac{1}{\epsilon_b}(\xi - \beta_0 - \rho + \epsilon_b \alpha_0) < \alpha_1^*.$$

Proof. The proof follows the same idea as in Lemma 7.2 i.e. a continuity argument for small ρ and the standard uniqueness result for ODEs applied to the planar slow flow on $S_{2,0}^{a-}$; see also Figure 7(b). \square

Now we may finish the proof for the second part of the main result.

Proof. (of Theorem 2.2, jump case and final result) The same steps as in the proof of the canard case in Section 7.1 can be applied upon noticing the following aspects:

- We always have $\beta_1 = \xi$.
- Applying the case (C4) from Proposition 3.10 is still valid due to Corollary 3.12.
- Instead of the canard case, we have to apply the jump case of Proposition 4.2.
- The b -direction contraction from Lemma 7.2 is replaced by Lemma 7.3.

As the remaining elements of the jump case proof are similar, we do not provide the details here. To conclude that there is indeed an open set of μ -values for the which the canard and jump case can be obtained, just via a variation of δ , we may apply Corollary 6.3. \square

8 Outlook

In addition to the non-classical relaxation oscillations described in Theorem 2.2, there are several other dynamical regimes of interest in the Olsen model. We do not provide the full details here and just give a brief geometric description of the other two cases observed by Olsen as shown in Figure 1.

We start with the case of MMOs. Part of the basic idea how MMOs may be generated can be found in [15]. However, with the results developed in this paper, we can already give a substantially more detailed description.

First, we observe that $k_1 = 0.16$ corresponds to the case in Table (2), where ϵ_b is also a small parameter. On a formal level, we still start with the system (6), and note that the reasonable assumption $\epsilon_b \epsilon \ll \epsilon_b$ implies that x is still the fastest variable and we may reduce the situation to a “slow” vector field on the normally hyperbolic part of \mathcal{C}_0 . This vector field is still solvable explicitly with $0 < \epsilon_b \ll 1$ as discussed in Section 5; see also Figure 8(a). The blow-up analysis in Section (3) has to be re-considered as we have to append $\epsilon'_b = 0$. Let us assume, i.e. we do not prove this conjecture here, that the main dynamical generating mechanism for the slowest dynamics is governed by the system (3), where ϵ_b is now another small parameter. Then (3) can be viewed as a fast-slow system with 3 fast variables and 1 slow variable. The critical manifold for this system is given by solving the algebraic equations

$$\begin{aligned} 0 &= \mu - \alpha a_2 - a_2 b_2 y_2, \\ 0 &= b_2 x_2 - x_2^2 + 3a_2 b_2 y_2 - \xi x_2, \\ 0 &= x_2^2 - y_2 - a_2 b_2 y_2, \end{aligned} \tag{75}$$

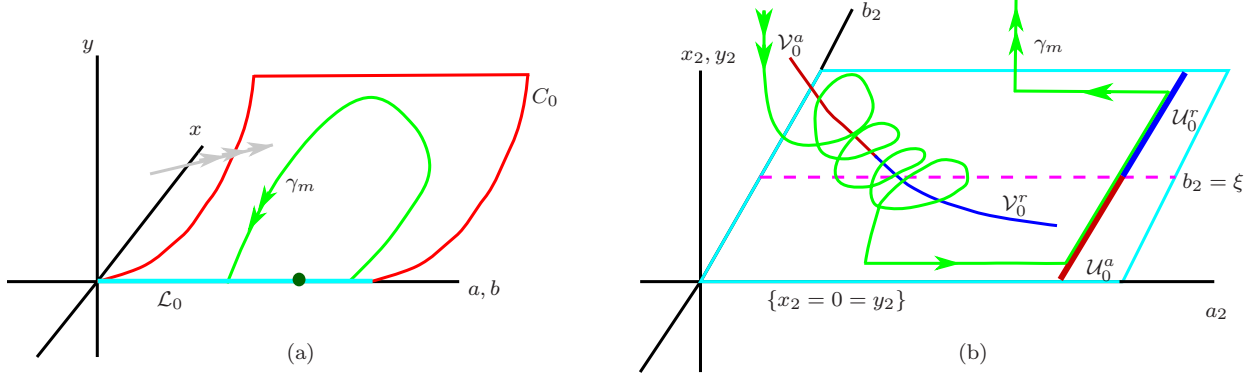


Figure 8: Sketch of the basic geometry for MMOs inside the region \mathcal{D} under the assumption $\epsilon_b \rightarrow 0$. (a) Phase space for the system (6) which captures the large fast loops. The critical manifold C_0 (red), two segments of an MMO candidate orbit γ_m (green), the fold manifold \mathcal{L}_0 (cyan), the submanifold $\{2ab = 1, x = 0 = y\}$ (dark-green dot) and the “super-fast” attracting dynamics (grey triple arrow) are shown. (b) Phase space for (6) with $\epsilon_b \rightarrow 0$. The focus is on the slow drift near \mathcal{L}_0 (cyan) and the “super-slow” dynamics near the critical manifold $\mathcal{U}_0 = \{a_2 = \mu/\alpha\}$ of (35). The candidate orbit γ_m (green), the exchange-of-stability line $\{b_2 = \xi\}$ (magenta) and the one-dimensional critical manifold \mathcal{V}_0 of (3) are shown; note that $\mathcal{V}_0 \cap \{x_2 = 0 = y_0\} = \emptyset$ i.e. \mathcal{V}_0 lies entirely above the submanifold $\{x_2 = 0 = y_0\}$. Furthermore, the two one-dimensional parts of the critical manifold split attracting (dark red) and repelling (blue) parts as $\mathcal{U}_0 = \mathcal{U}_0^a \cup \mathcal{U}_0^r$ and $\mathcal{V}_0 = \mathcal{V}_0^a \cup \mathcal{V}_0^r$. For a description of the dynamics please refer to the text in Section 8.

where we have assumed that $\delta = 0$ for convenience. The critical manifold described by (75) is given by one-dimensional curves. One part is given by

$$\mathcal{V}_0 := \left\{ x_2 = 0 = y_2, a_2 = \frac{\mu}{\alpha} \right\} = \mathcal{V}_0^a \cup p_{\mathcal{V}} \cup \mathcal{V}_0^r,$$

where $p_{\mathcal{V}} = \{b_2 = \xi, x_2 = 0 = y_2, a_2 = \frac{\mu}{\alpha}\}$, $\mathcal{V}_0^a = \mathcal{V}_0 \cap \{b_2 < \xi\}$ and $\mathcal{V}_0^r = \mathcal{V}_0 \cap \{b_2 > \xi\}$; see also Figure 8(b). \mathcal{V}_0^a is normally hyperbolic attracting, \mathcal{V}_0^r is normally hyperbolic repelling and $p_{\mathcal{V}}$ is not normally hyperbolic. Furthermore, there exists another curve

$$\mathcal{U}_0 = \mathcal{U}_0^a \cup p_{\mathcal{U}} \cup \mathcal{U}_0^r \subset \mathcal{S}_{2,0}^{a+} \cup \{b_2 = \xi, 2a_2\xi = 1\} \cup \mathcal{S}_{2,0}^{r-}$$

as shown in Figure 8(b), where $\mathcal{S}_{2,0}^{a+}$ and $\mathcal{S}_{2,0}^{r-}$ are the two-dimensional critical manifolds illustrated and discussed in Section 3.2 and illustrated in Figure 5. In particular, \mathcal{U}_0 also consists of three parts where one may check that $\mathcal{U}_0^a \subset \{b_2 > \xi\}$ is normally hyperbolic attracting with a linearization of the the fast subsystem having a real negative eigenvalue and a pair of complex conjugate eigenvalues with negative real parts. $\mathcal{U}_0^r \subset \{b_2 < \xi\}$ is normally hyperbolic repelling with a linearization of the the fast subsystem having a real negative eigenvalue and a pair of complex conjugate eigenvalues with positive real parts. A (delayed) Hopf bifurcation [58, 59] occurs at $p_{\mathcal{U}}$. This mechanism generates SAOs via a tourbillon-type mechanism [14] as trajectories spiral around \mathcal{U}_0 ; see also Figure 8(b). More precisely, after a large loop, trajectories spiral towards \mathcal{U}_0^a , including a slow drift towards $p_{\mathcal{U}}$. After the delayed Hopf bifurcation, trajectories spiral outwards around \mathcal{U}_0^r .

Then, we note that $\{x_2 = 0 = y_2\}$ is still invariant. Since ϵ_b is now viewed as a singular perturbation parameter, we can try to approximate the transition near $\{x_2 = 0 = y_2\}$ towards \mathcal{V}_0^a via the one-dimensional system

$$\frac{da_2}{ds} = \mu - \alpha a_2,$$

which is just (35) for $\epsilon_b = 0$. Trajectories reach a neighbourhood of \mathcal{V}_0^a and then drift slowly towards p_V . One has to prove an analogous result to the transcritical passage in Section 4 near p_V . Trajectories eventually leave \mathcal{V}_0^r and start another large loop as shown in Figure 8(b). A periodic orbit corresponds to an MMO as shown in Figure 1(a).

Although the description of MMOs we have just given is clearly not rigorous, the geometric structure suggested by Figure 8 indicates that a similar strategy as carried out in Sections 3-7 could work to prove the existence of MMOs. This problem is left open and could be considered in future work.

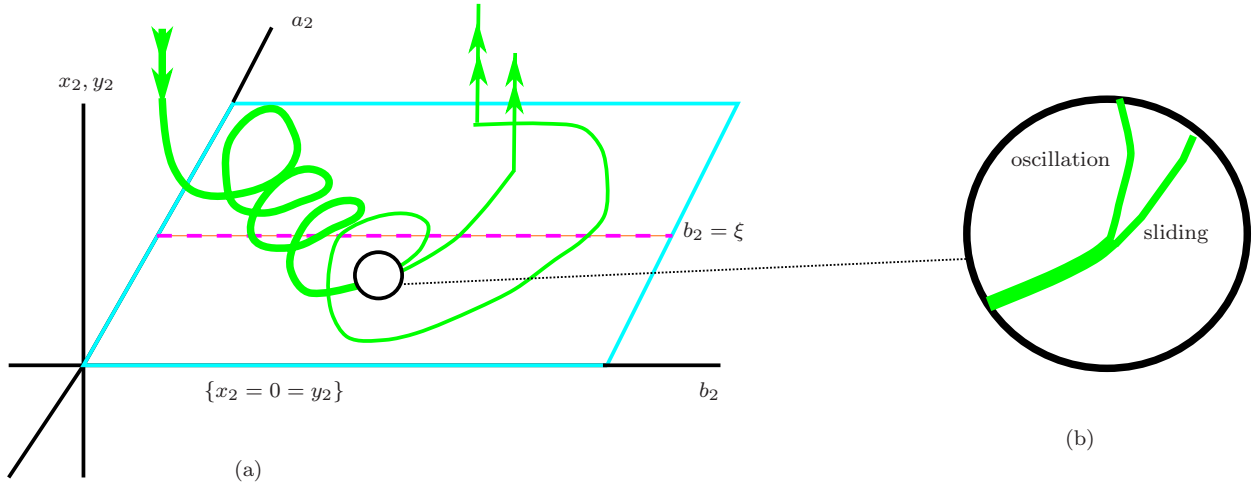


Figure 9: Sketch of the geometry for a possible chaos generating mechanism in the Olsen model. (a) Phase space for (6) in the intermediate regime between the non-classical relaxation oscillation case in Figure 2 and the MMO case in Figure 8. The focus is on the slow drift near \mathcal{L}_0 (cyan). (b) Sketch of the mechanism which causes the strong stretching of trajectories. One part of the orbits tend to make one more oscillation similar to the MMO case. The second part starts to “slide” on the set $\{x_2 = 0 = y_2\}$ similar to the non-classical relaxation oscillation case. For a more detailed description of the dynamics please refer to the text in Section 8.

The time series in Figure 1 suggest that there is an intermediate case between the regime of MMOs and the non-classical relaxation oscillations, where the Olsen model is chaotic; in particular, see Figure 1(b).

Several chaos-generating mechanism have been identified for fast-slow systems. We briefly recall two cases for classical relaxation oscillation system in \mathbb{R}^3 . One possibility is that jumps from a fold curve land on an attracting slow manifold where the slow flow has a tangency to the projection of the fold curve along the fast direction [41]. It has been shown in [27]

that there exists a near one-dimensional return map which is similar to a Hénon-type map. However, the basic mechanism for the flow to generate sensitive dependence upon initial conditions is that near the tangency orbits are “split” into different directions. Another possible chaos-generating mechanism has been identified in [29] based upon canard orbits arising from a folded saddle. In this context, there is also a “splitting”-type mechanism. Orbits follow the same canard but jump into different directions when departing from it, as well as departing from the fold curve where the fold saddle is based.

For both mechanisms, there is a region of phase space, where orbits are drastically separated. In combination with a global return mechanism, one obtains the main ingredients (stretching and folding) for Smale horseshoe dynamics [27, 29].

The Olsen model seems to exhibit a different mechanism, which also induces the drastic separation of orbits in part of the phase space. Figure 9 provides a basic sketch of the mechanism which we conjecture. Consider the singular limit $\epsilon = 0 = \epsilon_b$. Then there exists a family of fast subsystem periodic orbits around the repelling critical manifold \mathcal{V}_0^r which may become tangent to the invariant submanifold $\{x_2 = 0 = y_2\}$. If the system operates in a parameter regime between MMOs and non-classical relaxation oscillations, it could happen that a bundle of trajectories spirals in a region where \mathcal{V}_0^r (and $\mathcal{S}_{2,0}^{r-}$) are located. During their last SAO before reaching a neighbourhood of $\{x_2 = 0 = y_2\}$ some orbits may make one additional SAO, while others will tend to “slide” immediately towards $\{b_2 = \xi\}$; see Figure 9. This effect may cause the separation effect required to obtain a Smale horseshoe. The global returns are still controlled via \mathcal{C}_0 . Let us note that this mechanism also shares some similarities with grazing-sliding bifurcations of periodic orbits discussed recently in the context of non-smooth dynamical systems [16]. We are going to make this relation, and the chaos generating mechanism itself, more precise in future work.

In summary, we have given a precise description of the geometric structure and local asymptotic stability of non-classical relaxation oscillations originally discovered by Olsen more than 30 years ago. In particular, we have seen how the interaction between the two perturbation parameters ϵ and δ can be exploited to provide a coherent picture for the original numerical simulations as well as numerical continuation results obtained in [15] for a case between $\delta = 0$ and $\delta = K_2\epsilon^2$. Furthermore, we have briefly outlined how the analysis could be continued to cover the MMO and chaotic cases. The difficulty of the analysis shows that multiple time scale systems, which are not in standard form and possess several singular perturbation parameters, provide an interesting challenge for geometric singular perturbation theory.

Acknowledgments: CK would like to thank the Austrian Academy of Sciences (ÖAW) for support via an APART fellowship. CK and PS would like to thank the European Commission (EC/REA) for support by a Marie-Curie International Re-integration Grant.

A Normally Hyperbolicity & Fast-Slow Systems

We only recall the basic definitions and results about fast-slow systems. There are several standard references that detail many parts of the theory [38, 40, 57, 14, 3]. A fast-slow system of ordinary differential equations (ODEs) is given by:

$$\begin{aligned}\epsilon \dot{x} &= \epsilon \frac{dx}{d\tau} = f(x, y, \epsilon), \\ \dot{y} &= \frac{dy}{d\tau} = g(x, y, \epsilon),\end{aligned}\tag{76}$$

where $x \in \mathbb{R}^m$ are fast variables, $y \in \mathbb{R}^n$ are slow variables and $0 < \epsilon \ll 1$ is a small parameter representing the ratio of time scales. The maps f, g are assumed to be sufficiently smooth. Equation (76) can be re-written by changing from the slow time scale τ to the fast time scale $t = \tau/\epsilon$

$$\begin{aligned}x' &= \frac{dx}{dt} = f(x, y, \epsilon), \\ y' &= \frac{dy}{dt} = \epsilon g(x, y, \epsilon).\end{aligned}\tag{77}$$

The singular limit $\epsilon \rightarrow 0$ of (77) yields the fast subsystem ODEs parametrized by the slow variables y . Setting $\epsilon \rightarrow 0$ in (76) gives a differential-algebraic equation (DAE), called the slow subsystem, on the critical manifold $\mathcal{C}_0 := \{(x, y) \in \mathbb{R}^{m+n} : f(x, y, \epsilon) = 0\}$. Concatenations of fast and slow subsystem trajectories are called candidates [6, 29].

A subset $\mathcal{S} \subset \mathcal{C}$ is called normally hyperbolic if the $m \times m$ total derivative matrix $(D_x f)(p)$ is hyperbolic for $p \in \mathcal{S}$. A normally hyperbolic subset \mathcal{S} is attracting if all eigenvalues of $(D_x f)(p)$ have negative real parts for $p \in \mathcal{S}$, \mathcal{S} is called repelling if all eigenvalues have positive real parts and of saddle-type if there are positive and negative eigenvalues. On normally hyperbolic parts of \mathcal{C} the implicit function theorem applies to $f(x, y, 0) = 0$ providing a map $h_0(y) = x$ so that \mathcal{C} can be expressed (locally) as a graph.

Theorem A.1 (Fenichel's Theorem [21, 38, 71]). *Suppose $\mathcal{S} = \mathcal{S}_0$ is a compact normally hyperbolic submanifold (possibly with boundary) of the critical manifold \mathcal{C}_0 . Then, for $\epsilon > 0$ sufficiently small, there exists a locally invariant manifold \mathcal{S}_ϵ diffeomorphic to \mathcal{S}_0 . \mathcal{S}_ϵ has a distance of $\mathcal{O}(\epsilon)$ from \mathcal{S}_0 and the flow on \mathcal{S}_ϵ converges to the slow flow as $\epsilon \rightarrow 0$.*

The distance between \mathcal{S}_ϵ and \mathcal{S}_0 can be expressed in the Hausdorff metric or a suitable C^r -norm (using the map h_0 and its perturbation h_ϵ). A manifold \mathcal{S}_ϵ provided by Fenichel's Theorem is called a slow manifold. Slow manifolds are usually not unique but different slow manifolds lie at a distance $\mathcal{O}(e^{-K/\epsilon})$ for some constant $K > 0$. Often we shall make a choice of compact subset and choice of slow manifold without further notice, indicating that the choice does not matter for the asymptotic analysis performed.

A trajectory is called a maximal canard if it lies in the intersection of an attracting and a repelling slow manifold. Canards were first investigated by a group of French mathematicians [7] using nonstandard analysis. Later also asymptotic [20, 4] and geometric [19, 45] methods have been developed to understand canard orbits.

B Geometric Desingularization

Here we shall briefly review the basic strategy for the blow-up approach for geometric desingularization of fast-slow systems. Details on the classical, single-scale, method can be found

e.g. in [18]. The classical blow-up was first introduced into fast-slow systems in [19]. Further developments can be found in [45]; see also the introduction in [47].

The starting point is to write the system (77) as follows

$$\begin{aligned} x' &= f(x, y, \epsilon), \\ y' &= \epsilon g(x, y, \epsilon), \\ \epsilon' &= 0. \end{aligned} \tag{78}$$

Let us denote the vector field defined by (78) as X i.e. X is a mapping

$$X : \mathbb{R}^{m+n} \times [0, \epsilon_0) \rightarrow T(\mathbb{R}^{m+n} \times [0, \epsilon_0))$$

where $T(\cdot)$ indicates the tangent bundle. Further equations for parameters could be appended to (78) as well, if necessary. Suppose (78) has an equilibrium point for $\epsilon = 0$, or more generally a submanifold $\mathcal{M} = \{f = 0\}$ of equilibria in $\mathbb{R}^{m+n} \times \{\epsilon = 0\}$. If $(D_x f)(p)$ is not a hyperbolic matrix for each $p \in \mathcal{M}$, the equilibrium (manifold) \mathcal{M} is degenerate and classical linearization results do not apply directly to (78).

The blow-up technique is based upon replacing \mathcal{M} by a, usually more complicated, manifold $\bar{\mathcal{M}}$ and using a map

$$\Phi : \bar{\mathcal{M}} \rightarrow \mathcal{M}$$

which induces a vector field \bar{X} on $\bar{\mathcal{M}}$ via the pushforward Φ_* and the condition $\Phi_*(\bar{X}) = X$. Using a good choice for $\bar{\mathcal{M}}$, one may often analyze the blown-up vector field \bar{X} as it is possible that invariant manifolds of \bar{X} are now (partially) hyperbolic.

As an example, consider the classical case when $(x, y) \in \mathbb{R}^2$ and $f(x, y) = y - x^2$ is the (truncated) normal form of a fold bifurcation. The origin $(x, y, \epsilon) = (0, 0, 0)$ is the important non-hyperbolic point and the standard choice is to use a sphere for geometric desingularization $\bar{\mathcal{M}} := S^2 \times [0, r_0)$ for some constant $r_0 > 0$ or $r_0 = +\infty$. Therefore, one has essentially inserted a sphere at the origin; see also [19, 47].

Although one could try to find a suitable global parametrization of $\bar{\mathcal{M}}$, this is usually not very convenient for calculations. Instead, one uses charts $\kappa_j : \bar{\mathcal{M}} \rightarrow \mathbb{R}^{m+n+1}$ of $\bar{\mathcal{M}}$ for the calculations, which is illustrated by the following important diagram

$$\begin{array}{ccc} & \bar{\mathcal{M}} & \\ \kappa_j \swarrow & & \searrow \Phi \\ \mathbb{R}^{m+n+1} & \xrightarrow{\varphi_j} & \mathbb{R}^{m+n+1} \end{array}$$

which commutes. Hence, one may just try to calculate the map φ_j and obtain a vector field on \mathbb{R}^{m+n+1} by applying the coordinate change

$$(x_j, y_j, \epsilon_j) = \varphi^{-1}(x, y, \epsilon).$$

One may often, via a good choice of $\bar{\mathcal{M}}$ and chart maps κ_j , compute the vector fields in (x_j, y_j, ϵ_j) -coordinates. The same remark applies to the transition maps between different charts κ_{jk} . Section 3 carries out these calculations for a submanifold of fold points in the Olsen model.

C An Auxiliary Center Manifold Reduction

Here we present the details for the center manifold calculation for (27). We drop the sub- and superscripts of (r_1, y_1, ϵ_1) and (α_1^*, b_1^*) for notational convenience; all variables and constants used in this section are temporary and should not be confused with notation within the main manuscript. Re-ordering the variables and translating (27) via $Y = y - 1/(3ab)$ yields

$$\begin{aligned} r' &= r [\epsilon(b - \xi) + 3abY] =: f_1(r, \epsilon, Y), \\ \epsilon' &= -\epsilon [\epsilon(b - \xi) + 3abY] =: f_2(r, \epsilon, Y) \\ Y' &= f_3(r, \epsilon, Y), \end{aligned} \tag{79}$$

where the function f_3 is given by

$$f_3(r, \epsilon, Y) := \kappa\epsilon(1 - [Y + 1/(3ab)][1 + a_1^*b_1^*]) - 2[Y + 1/(3ab)](\epsilon(b - \xi) + 3aby).$$

Let $z := (r, \epsilon, Y)^T$ and consider

$$A := D_z(z')|_{(0,0,0)} = \begin{pmatrix} 0 & 0 & 0 \\ 0 & 0 & 0 \\ 0 & K & -2 \end{pmatrix} \quad \text{and} \quad M := \begin{pmatrix} 1 & 0 & 0 \\ 0 & -2/K & 0 \\ 0 & 1 & 1 \end{pmatrix},$$

where $K := -(2b + \kappa - 2ab\kappa - 2\xi)/(3ab)$. Let $(x_1, x_2, \tilde{y})^T = \tilde{z} = M^{-1}z$ and observe that $M^{-1}AM = J \in \mathbb{R}^{3 \times 3}$ with $J_{33} = -2$ and $J_{ij} = 0$ otherwise. Set $\tilde{z} = (x_1, x_2, \tilde{y}) = M^{-1}z$ so that

$$\begin{aligned} \begin{pmatrix} x'_1 \\ x'_2 \\ \tilde{y}' \end{pmatrix} &= \begin{pmatrix} 0 & 0 \\ 0 & 0 \end{pmatrix} \begin{pmatrix} x_1 \\ x_2 \end{pmatrix} + \begin{pmatrix} F_1(x_1, x_2, \tilde{y}) \\ F_2(x_1, x_2, \tilde{y}) \\ G(x_1, x_2, \tilde{y}) \end{pmatrix} \end{aligned} \tag{80}$$

where $(F_1, F_2, G)^T = (0, 0, 2\tilde{y})^T + M^{-1}(f_1(M\tilde{z}), f_2(M\tilde{z}), f_3(M\tilde{z}))^T$. The system (80) is in the standard form for center manifold theory [25]. The usual perturbation ansatz is $\tilde{y} = h(x_1, x_2) = k_{11}x_1^2 + k_{12}x_1x_2 + k_{22}x_2^2 + \mathcal{O}(3)$, where $\mathcal{O}(3) := \mathcal{O}(x_1^3, x_1^2x_2, x_1x_2^2, x_2^3)$. The defining invariance equation for the center manifold with $x = (x_1, x_2)^T$ and $F = (F_1, F_2)^T$ is

$$Dh(x)F(x, h(x)) = -2h(x) + G(x, h(x)) \tag{81}$$

since the x' -equations in (80) have no linear term. Collecting terms of order $\mathcal{O}(x_1^2)$ in (81) gives $k_{11} = 0$ and the $\mathcal{O}(x_1x_2)$ -terms give $k_{12} = 0$. For $\mathcal{O}(x_2^2)$ equation (81) and $k_{11} = 0 = k_{12}$ imply

$$k_{22} = \frac{3ab(1 + 4ab)\kappa}{4(b - \xi) + 2\kappa(1 - 2ab)}.$$

Transforming back to the variables (r, ϵ, y) via the matrix M and translation yields the center manifold

$$y = \frac{1}{3ab} + \epsilon \frac{2(\xi - b) + \kappa(2ab - 1)}{6ab} + k_{22} \frac{K^2}{4} \epsilon^2 + \mathcal{O}(3),$$

where $\mathcal{O}(3) = \mathcal{O}(r^3, r^2\epsilon, r\epsilon^2, \epsilon^3)$. Computing

$$k_{22} \frac{K^2}{4} = \frac{\kappa(1 + 4ab)}{24ab} (2(b - \xi) + \kappa(1 - 2ab))$$

yields Proposition 3.9.

D Another Auxiliary Center Manifold Reduction

As for the center manifold reduction in Appendix C we present some of the important details for the center manifold calculation. As before for the previous appendix, the notation here only pertains to this calculation and should not be confused with variables within the main text. It is convenient to translate (33) via $B_2 := b_2 - \xi$, to re-label $x_2 = X_2$, $y_2 = Y_2$ and change to the time scale $\tau = s/\epsilon^2$ which yields

$$\begin{aligned}\dot{X}_2 &= 3a_2(B_2 + \xi)Y_2 - X_2^2 + B_2X_2 + \delta, \\ \dot{a}_2 &= \epsilon^2(\mu - \alpha a_2 - a_2(B_2 + \xi)Y_2), \\ \dot{B}_2 &= \epsilon^2\epsilon_b(1 - (B_2 + \xi)X_2 - a_2(B_2 + \xi)Y_2), \\ \dot{\epsilon} &= 0, \\ \dot{\delta} &= 0, \\ \dot{Y}_2 &= \kappa(X_2^2 - Y_2 - a_2(B_2 + \xi)Y_2).\end{aligned}\tag{82}$$

The system (82) has a line of equilibrium points

$$\mathcal{E}_2 := \{(X_2, a_2, B_2, \epsilon, \delta, Y_2) = (0, a_2, 0, 0, 0, 0)\},$$

which is degenerate since the linearization of (82) at \mathcal{E}_2 for fixed $a_2 = a_0$ is

$$A = D_{(X_2, a_2, b_2, \epsilon, \delta, Y_2)} \begin{pmatrix} \dot{X}_2 \\ \dot{a}_2 \\ \dot{B}_2 \\ \dot{\epsilon} \\ \dot{\delta} \\ \dot{Y}_2 \end{pmatrix} \bigg|_{\mathcal{E}_2} = \begin{pmatrix} 0 & 0 & 0 & 0 & 1 & 3a_0\xi \\ 0 & 0 & 0 & \mu - \alpha a_0 & 0 & 0 \\ 0 & 0 & 0 & \epsilon_b & 0 & 0 \\ 0 & 0 & 0 & 0 & 0 & 0 \\ 0 & 0 & 0 & 0 & 0 & 0 \\ 0 & 0 & 0 & 0 & 0 & -\kappa(1 + a_0\xi) \end{pmatrix}. \tag{83}$$

This matrix has one negative eigenvalue $-\kappa(1 + a_0\xi)$ and a quintuple zero eigenvalue. Hence a center manifold reduction to a five-dimensional center flow is required to resolve the dynamics near \mathcal{E}_2 . However, we use a preliminary transformation to get the system into standard form. Let $Z = (X_2, Y_2)^T$ and set

$$A_{XY} := \begin{pmatrix} 0 & 3a_0\xi \\ 0 & -\kappa(1 + a_0\xi) \end{pmatrix} \quad \text{and} \quad M := \begin{pmatrix} 1 & -\frac{3a_0\xi}{\kappa(1 + a_0\xi)} \\ 0 & 1 \end{pmatrix}.$$

Then consider new coordinates via $M\tilde{Z} = Z$ and observe that in the coordinates $(\tilde{X}_2, \tilde{Y}_2)^T$ we have

$$\tilde{Z}' = M^{-1}A_{XY}M\tilde{Z} + \text{h.o.t.} = \begin{pmatrix} 0 & 0 \\ 0 & -\kappa(1 + a_0\xi) \end{pmatrix} \begin{pmatrix} \tilde{X}_2 \\ \tilde{Y}_2 \end{pmatrix} + \text{h.o.t.},$$

where h.o.t. denotes higher-order terms. Let $x := (x_1, x_2, x_3, x_4, x_5) = (\tilde{X}_2, a_0 - a_2, b_2, \epsilon, \delta)$ so that $y = \tilde{Y}_2$ is the transformation of (82) into new coordinates

$$\begin{aligned} x'_1 &= x_5 + 3x_3y(x_3 + \xi) + x_3 \left(x_1 - \frac{3a_0y\xi}{\kappa + a_0\kappa\xi} \right) - \left(x_1 - \frac{3a_0y\xi}{\kappa + a_0\kappa\xi} \right)^2 \\ &\quad - 3a_0\xi \frac{y + (a_0 - x_2)y(x_3 + \xi) - \left(x_1 - \frac{3a_0y\xi}{\kappa + a_0\kappa\xi} \right)^2}{1 + a_0\xi}, \\ x'_2 &= x_4(\mu - (a_0 - x_2)(\alpha + y(x_3 + \xi))), \\ x'_3 &= x_4\epsilon_b(1 - (a_0 - x_2)y(x_3 + \xi) - (x_3 + \xi) \left(x_1 - \frac{3a_0y\xi}{\kappa + a_0\kappa\xi} \right)), \\ x'_4 &= 0, \\ x'_5 &= 0, \\ y' &= \kappa \left(-y - (a_0 - x_2)y(x_3 + \xi) + \left(x_1 - \frac{3a_0y\xi}{\kappa + a_0\kappa\xi} \right)^2 \right), \end{aligned}$$

which is a vector field we denote by $(Cx + F(x, y), Py + G(x, y))^T$ for $F(x, y) \in \mathbb{R}^5$, $G(x, y) \in \mathbb{R}$. Observe that

$$C = \{A_{ij}\}_{i,j=1}^5, \quad \text{and} \quad P = -\kappa(1 + a_0\xi).$$

The vector field is now in the correct form for center manifold theory, applied along the entire line of points parametrized by a_0 . The ansatz is

$$y = h(x) = \sum_{i+j=2, i \leq j} c_{ij} x_i x_j.$$

The usual invariance equation is given by

$$Dh(x)[Cx + F(x, h(x))] = Ph(x) + G(x, h(x)),$$

where different powers $x_i x_j$ have to have equal coefficients on both sides. This procedure yields

$$c_{11} = \frac{1}{1 + a_0\xi}, \quad c_{15} = -\frac{1}{\kappa(1 + a_0\xi)^2}, \quad c_{55} = -\frac{1}{\kappa^2(1 + a_0\xi)^3}.$$

All other coefficients c_{ij} have vanish. Hence the center manifold is given to lowest order by

$$\tilde{Y}_2 = \frac{\tilde{X}_2^2}{1 + a_0\xi} - \frac{\tilde{X}_2\delta}{\kappa(1 + a_0\xi)^2} - \frac{\delta^2}{\kappa^2(1 + a_0\xi)^3}. \quad (84)$$

Transforming back to original coordinates and keeping lowest order terms yields

$$Y_2 = \frac{X_2^2}{1 + a_0\xi} - \frac{\delta X_2}{\kappa(1 + a_0\xi)^2} + \frac{\delta^2}{\kappa^2(1 + a_0\xi)^3} + \mathcal{O}(Y_2^2, X_2^3, X_2 Y_2, \delta Y_2, \delta^3). \quad (85)$$

Substituting the result into (82) gives, up to leading order, the center flow

$$\begin{aligned} \epsilon^2 \frac{dX_2}{ds} &= X_2^2 \left(\frac{2a_0\xi - 1}{1 + a_0\xi} \right) + X_2 \left(\frac{-\delta}{\kappa(1 + a_0\xi)^2} + B_2 \right) + \delta + \frac{\delta^2}{\kappa^2(1 + a_0\xi)^3} + \mathcal{O}(3), \\ \frac{da_2}{ds} &= \mu - \alpha a_2 + \mathcal{O}(2), \\ \frac{dB_2}{ds} &= \epsilon_b + \mathcal{O}(2), \end{aligned} \quad (86)$$

which is precisely the result we wanted to prove.

References

- [1] B.D. Aguda and R. Larter. Periodic-chaotic sequences in a detailed mechanism of the peroxidase-oxidase reaction. *J. Am. Chem. Soc.*, 113:7913–7916, 1991.
- [2] B.D. Aguda, R. Larter, and B.L. Clarke. Dynamic elements of mixed-mode oscillations and chaos in a peroxidase-oxidase network. *J. Chem. Phys.*, 90(8):4168–4175, 1989.
- [3] V.I. Arnold. *Encyclopedia of Mathematical Sciences: Dynamical Systems V*. Springer, 1994.
- [4] S.M. Baer and T. Erneux. Singular Hopf bifurcation to relaxation oscillations I. *SIAM J. Appl. Math.*, 46(5):721–739, 1986.
- [5] D. Barkley. Slow manifolds and mixed-mode oscillations in the Belousov-Zhabotinskii reaction. *J. Chem. Phys.*, 89(9):5547–5559, 1988.
- [6] E. Benoît. Canards et enlacements. *Publ. Math. IHES*, 72:63–91, 1990.
- [7] E. Benoît, J.L. Callot, F. Diener, and M. Diener. Chasse au canards. *Collect. Math.*, 31:37–119, 1981.
- [8] T.V. Bronnikova, V.R. Fed’kina, W.M. Schaffer, and L.F. Olsen. Period-doubling bifurcations and chaos in a detailed model of the peroxidase-oxidase reaction. *J. Phys. Chem.*, 99(23):9309–9312, 1995.
- [9] T.V. Bronnikova, W.M. Schaffer, and L.F. Olsen. Nonlinear dynamics of the peroxidase-oxidase reaction. I. Bistability and bursting oscillations at low enzyme concentrations. *J. Phys. Chem. B*, 105:310–321, 2001.
- [10] M.L. Cartwright and J.E. Littlewood. On non-linear differential equations of second order. I. The equation $\ddot{y} - k(1 - y^2)\dot{y} + y = b\lambda k \cos(\lambda t + a)$, k large. *J. London Math. Soc.*, 20:180–189, 1945.
- [11] M.L. Cartwright and J.E. Littlewood. On non-linear differential equations of second order. II. The equation $\ddot{y} - kf(y, \dot{y}) + g(y, k) = p(t)$, $k > 0$, $f(y) \geq 1$. *Ann. Math.*, 48(2):472–494, 1947.
- [12] H. Chiba. Periodic orbits and chaos in fast-slow systems with Bogdanov-Takens type fold points. *J. Diff. Eq.*, 250:112–160, 2011.
- [13] H. Degn, L.F. Olsen, and J.W. Perram. Bistability, oscillation, and chaos in an enzyme reaction. *Annals of the New York Academy of Sciences*, 316(1):623–637, 1979.
- [14] M. Desroches, J. Guckenheimer, C. Kuehn, B. Krauskopf, H. Osinga, and M. Wechselberger. Mixed-mode oscillations with multiple time scales. *SIAM Rev.*, 54(2):211–288, 2012.
- [15] M. Desroches, B. Krauskopf, and H.M. Osinga. The geometry of mixed-mode oscillations in the Olsen model for the peroxidase-oxidase reaction. *DCDS-S*, 2(4):807–827, 2009.

- [16] M. di Bernardo, C.J. Budd, A.R. Champneys, and P. Kowalczyk. *Piecewise-smooth Dynamical Systems*, volume 163 of *Applied Mathematical Sciences*. Springer, 2008.
- [17] M. Diener. The canard unchained or how fast/slow dynamical systems bifurcate. *The Mathematical Intelligencer*, 6:38–48, 1984.
- [18] F. Dumortier. Techniques in the theory of local bifurcations: Blow-up, normal forms, nilpotent bifurcations, singular perturbations. In D. Schlomiuk, editor, *Bifurcations and Periodic Orbits of Vector Fields*, pages 19–73. Kluwer, Dordrecht, The Netherlands, 1993.
- [19] F. Dumortier and R. Roussarie. *Canard Cycles and Center Manifolds*, volume 121 of *Memoirs Amer. Math. Soc.* AMS, 1996.
- [20] W. Eckhaus. Relaxation oscillations including a standard chase on French ducks. *Lecture Notes in Mathematics*, 985:449–494, 1983.
- [21] N. Fenichel. Geometric singular perturbation theory for ordinary differential equations. *Journal of Differential Equations*, 31:53–98, 1979.
- [22] T. Geest, L.F. Olsen, C.G. Steinmetz, R. Larter, and Schaffer. Nonlinear analysis of periodic and chaotic time series from the peroxidase-oxidase reaction. *J. Phys. Chem.*, 97:8431–8441, 1993.
- [23] T. Geest, C.G. Steinmetz, R. Larter, and L.F. Olsen. Period-doubling bifurcations and chaos in an enzyme reaction. *J. Phys. Chem.*, 96:5678–5680, 1992.
- [24] J. Grasman. *Asymptotic Methods for Relaxation Oscillations and Applications*. Springer, 1987.
- [25] J. Guckenheimer and P. Holmes. *Nonlinear Oscillations, Dynamical Systems, and Bifurcations of Vector Fields*. Springer, New York, NY, 1983.
- [26] J. Guckenheimer and C. Scheper. A geometric model for mixed-mode oscillations in a chemical system. *SIAM J. Appl. Dyn. Sys.*, 10(1):92–128, 2011.
- [27] J. Guckenheimer, M. Wechselberger, and L.-S. Young. Chaotic attractors of relaxation oscillations. *Nonlinearity*, 19:701–720, 2006.
- [28] I. Gucwa and P. Szmolyan. Geometric singular perturbation analysis of an autocatalator model. *DCDS-S*, 2(4):783–806, 2009.
- [29] R. Haiduc. Horseshoes in the forced van der Pol system. *Nonlinearity*, 22:213–237, 2009.
- [30] E. Harvey, V. Kirk, H.M. Osinga, J. Sneyd, and M. Wechselberger. Understanding anomalous delays in a model of intracellular calcium dynamics. *Chaos*, 20:045104, 2010.
- [31] T. Hauck and F.W. Schneider. Mixed-mode and quasiperiodic oscillations in the peroxidase-oxidase reaction. *J. Phys. Chem.*, 97:391–397, 1993.

- [32] T. Hauck and F.W. Schneider. Chaos in a Farey sequence through period doubling in the peroxidase-oxidase reaction. *J. Phys. Chem.*, 98:2072–2077, 1994.
- [33] M.J.B. Hauser and L.F. Olsen. Mixed-mode oscillations and homoclinic chaos in an enzyme reaction. *J. Chem. Soc. Faraday Trans.*, 92(16):2857–2863, 1996.
- [34] M.J.B. Hauser, L.F. Olsen, T.V. Bronnikova, and W.M. Schaffer. Routes to chaos in the peroxidase-oxidase reaction: period-doubling and period-adding. *J. Phys. Chem. B*, 101:5075–5083, 1997.
- [35] M.W. Hirsch, C.C. Pugh, and M. Shub. *Invariant Manifolds*. Springer, 1977.
- [36] A. Huber and P. Szmolyan. Geometric singular perturbation analysis of the Yamada model. *SIAM J. Applied Dynamical Systems*, 4(3):607–648, 2005.
- [37] E. Izhikevich. Neural excitability, spiking, and bursting. *Int. J. Bif. Chaos*, 10:1171–1266, 2000.
- [38] C.K.R.T. Jones. Geometric singular perturbation theory. In *Dynamical Systems (Montecatini Terme, 1994)*, volume 1609 of *Lect. Notes Math.*, pages 44–118. Springer, 1995.
- [39] T.J. Kaper. An introduction to geometric methods and dynamical systems theory for singular perturbation problems. analyzing multiscale phenomena using singular perturbation methods. In J. Cronin and R.E. O’Malley, editors, *Analyzing Multiscale Phenomena Using Singular Perturbation Methods*, pages 85–131. Springer, 1999.
- [40] T.J. Kaper and C.K.R.T. Jones. A primer on the exchange lemma for fast-slow systems. In *Multiple-Time-Scale Dynamical Systems*, pages 65–88. Springer, 2001.
- [41] E.F. Mishchenko Yu.S. Kolesov, A.Yu. Kolesov, and N.Kh. Rozov. *Asymptotic Methods in Singularly Perturbed Systems*. Plenum Press, 1994.
- [42] I. Kosiuk and P. Szmolyan. Scaling in singular perturbation problems: blowing-up a relaxation oscillator. *SIAM J. Appl. Dyn. Syst.*, 10(4):1307–1343, 2011.
- [43] I. Kosiuk and P. Szmolyan. A new type of relaxation oscillations in a model of the mitotic oscillator. *preprint*, 2013.
- [44] M. Krupa, N. Popovic, and N. Kopell. Mixed-mode oscillations in three time-scale systems: A prototypical example. *SIAM J. Appl. Dyn. Syst.*, 7(2):361–420, 2008.
- [45] M. Krupa and P. Szmolyan. Extending geometric singular perturbation theory to non-hyperbolic points - fold and canard points in two dimensions. *SIAM J. Math. Anal.*, 33(2):286–314, 2001.
- [46] M. Krupa and P. Szmolyan. Extending slow manifolds near transcritical and pitchfork singularities. *Nonlinearity*, 14:1473–1491, 2001.
- [47] M. Krupa and P. Szmolyan. Geometric analysis of the singularly perturbed fold. *in: Multiple-Time-Scale Dynamical Systems*, IMA Vol. 122:89–116, 2001.

- [48] M. Krupa and P. Szmolyan. Relaxation oscillation and canard explosion. *J. Differential Equat.*, 174:312–368, 2001.
- [49] M. Krupa, A. Vidal, M. Desroches, and F. Clément. Mixed-mode oscillations in a multiple time scale phantom bursting system. *SIAM J. Appl. Dyn. Syst.*, 11(4):1458–1498, 2012.
- [50] C. Kuehn. On decomposing mixed-mode oscillations and their return maps. *Chaos*, 21(3):033107, 2011.
- [51] C. Kuehn. Loss of normal hyperbolicity of unbounded critical manifolds. *arXiv:1204.0947v3*, pages 1–15, 2013.
- [52] R. Larter, C.L. Bush, T.R. Lonis, and B.D. Aguda. Multiple steady states, complex oscillations, and the devil’s staircase in the peroxidase-oxidase reaction. *J. Chem. Phys.*, 87(10):5765–5771, 1987.
- [53] R. Larter and S. Hemkin. Further refinements of the peroxidase-oxidase oscillator mechanism: Mixed-mode oscillations and chaos. *J. Phys. Chem.*, 100:18924–18930, 1996.
- [54] R. Larter and C.G. Steinmetz. Chaos via mixed-mode oscillations. *Phil. Trans. R. Soc. Lond. A*, 337:291–298, 1991.
- [55] D. Liu. Exchange lemmas for singular perturbation problems with certain turning points. *J. Differential Equat.*, 167:134–180, 2000.
- [56] A. Milik. *Mixed-mode oscillations in chemical systems*. PhD thesis, Vienna University of Technology, Vienna, Austria, 1998.
- [57] E.F. Mishchenko and N.Kh. Rozov. *Differential Equations with Small Parameters and Relaxation Oscillations (translated from Russian)*. Plenum Press, 1980.
- [58] A.I. Neishtadt. Persistence of stability loss for dynamical bifurcations. I. *Differential Equations Translations*, 23:1385–1391, 1987.
- [59] A.I. Neishtadt. Persistence of stability loss for dynamical bifurcations. II. *Differential Equations Translations*, 24:171–176, 1988.
- [60] L.F. Olsen. An enzyme reaction with a strange attractor. *Physics Letters A*, 94(9):454–457, 1983.
- [61] L.F. Olsen and H. Degn. Oscillatory kinetics of the peroxidase-oxidase reaction in an open system. Experimental and theoretical studies. *Biochim. Biophys. Acta*, 523(2):321–334, 1978.
- [62] D.L. Olson, E.P. Williksen, and A. Scheeline. An experimentally based model of the Peroxidase-NADH biochemical oscillator: An enzyme-mediated chemical switch. *J. Am. Chem. Soc.*, 117:2–15, 1995.

- [63] J. Rinzel. A formal classification of bursting mechanisms in excitable systems. *Proc. Int. Congress Math., Berkeley*, pages 1578–1593, 1986.
- [64] W.M. Schaffer, T.V. Bronnikova, and L.F. Olsen. Nonlinear dynamics of the peroxidase-oxidase reaction. II. Compatibility of an extended model with previously reported model-data correspondences. *J. Phys. Chem.*, 105:5331–5340, 2001.
- [65] S. Schechter. Exchange lemmas 2: general exchange lemma. *J. Differential Equat.*, 245(2):411–441, 2008.
- [66] A. Scheeline, D.L. Olson, E.P. Williksen, G.A. Horras, M.L. Klein, and R. Larter. The peroxidase-oxidase oscillator and its constituent chemistries. *Chem. Rev.*, 97:739–756, 1997.
- [67] C.G. Steinmetz, T. Geest, and R. Larter. Universality in the peroxidase-oxidase reaction: period doublings, chaos, period three, and unstable limit cycles. *J. Phys. Chem.*, 97:5649–5653, 1993.
- [68] C.G. Steinmetz and R. Larter. The quasiperiodic route to chaos in a model of the peroxidase-oxidase reaction. *J. Phys. Chem.*, 94(2):1388–1396, 1991.
- [69] P. Szmolyan and M. Wechselberger. Canards in \mathbb{R}^3 . *J. Differential Equat.*, 177:419–453, 2001.
- [70] D.R. Thompson and R. Larter. Multiple time scale analysis of two models for the peroxidase-oxidase reaction. *Chaos*, 5(2):448–457, 1995.
- [71] A.N. Tikhonov. Systems of differential equations containing small parameters in the derivatives. *Mat. Sbornik N. S.*, 31:575–586, 1952.
- [72] B. van der Pol. A theory of the amplitude of free and forced triode vibrations. *Radio Review*, 1:701–710, 1920.
- [73] B. van der Pol. On relaxation oscillations. *Philosophical Magazine*, 7:978–992, 1926.
- [74] M. Wechselberger. A propos de canards (apropos canards). *Trans. Amer. Math. Soc.*, 364:3289–3309, 2012.

Contents

| | | |
|----------|---|-----------|
| 1 | Introduction & Review | 1 |
| 2 | Transformations and the Main Result | 4 |
| 3 | The Main Blow-Up | 9 |
| 3.1 | First Chart | 12 |
| 3.2 | Second Chart | 16 |
| 4 | Transcritical Singularities | 19 |
| 5 | Large Loops | 23 |
| 6 | Construction of Candidate Orbits | 25 |
| 6.1 | A Canard Candidate | 25 |
| 6.2 | A Jump Candidate | 28 |
| 7 | The Return Map | 29 |
| 7.1 | The Canard Case | 29 |
| 7.2 | The Jump Case | 32 |
| 8 | Outlook | 33 |
| A | Normally Hyperbolicity & Fast-Slow Systems | 37 |
| B | Geometric Desingularization | 37 |
| C | An Auxiliary Center Manifold Reduction | 39 |
| D | Another Auxiliary Center Manifold Reduction | 40 |